Investigating the consequences of substituting histidine ligands to hemes in the decaheme cytochrome MtrC

Keir Whiting

A Thesis for the degree of Master of Science by Research

University of East Anglia, Norwich, UK

School of Chemistry

August 2024

I certify that I have read this dissertation and that, in my opinion, it is fully adequate in scope and quality as a dissertation for the degree of Master of Science by Research

X_____

Abstract

MtrC is a decaheme *c*-type cytochrome found naturally on the external face of the outer membrane of *Shewanella oneidensis* MR-1. Previous studies have prepared a soluble version of this protein containing a surface tyrosine to cysteine (Y657C) substitution that can be photosensitised with a Ru(II)bipyridine$_3$ dye. This surface mounted dye allowed for pump-probe spectroscopy experiments to measure electron transfer rates across MtrC. In the same experiments the substitution of a distal histidine ligand to heme eight with a methionine residue increased the lifetime of the charge separated state. This work discusses the production and characterisation of two additional heme distal ligand substitutions, a heme eight histidine to cysteine (H561C) substitution, and a heme three histidine to methionine (H230M) substitution. Electronic absorbance and magnetic circular dichroism spectroscopies revealed all hemes in solution are low-spin, consistent with octahedral coordination of all iron centres. X-ray crystallographic structures of the H230M variant confirmed the sulphur of methionine 230 to be the distal ligand to heme three. However, the crystal structure of the H561C variant revealed the distal ligand to heme eight is not the sulphur of cysteine 561, but a post translational covalent modification to the cysteine. This covalent modification is likely to represent the ligand in solution as liquid chromatography-mass spectrometry revealed a homogeneous population with a mass of +51 Da higher than anticipated. Protein film electrochemical measurements reveal that both the H230M and H561C variants exhibit shifts in the macroscopic redox potential of one or more redox centres in the proteins. These findings offer the opportunity to explore the impact on the charge separated lifetime of the photosensitised proteins during pump-probe spectroscopy, as well as offering new ways to study electron transfer dynamics in multiheme cytochromes through introduction of unique spectroscopic centres.

Table of Contents

Abbreviations

ATP	Adenosine triphosphate
CD	Circular dichroism
EDTA	Ethylenediaminetetraacetic acid
EPR	Electro paramagnetic resonance
ITO	Indium tin oxide
$K_3Fe(CN)_6$	Potassium ferricyanide
LB	Lysogeny broth
LC-MS	Liquid chromatography-mass spectrometry
M72 Media	NaCl (5 g/L) Papaic digest of soybean meal (5 g/L) Casein digest of peptone (15 g/L)
M72 Media additions	Sodium D, L-lactate (20 mM) Sodium fumarate (20 mM) HEPES (20 mM)
NaDT	Sodium dithionite
NIR-MCD	Near infrared-magnetic circular dichroism
PCR	Polymerase chain reaction
Ru-MtrC	MtrC protein labelled with a Ru(II)bipyridine$_3$ dye
SDS-PAGE	Sodium dodecyl sulphate-polyacrylamide gel electrophoresis
SHE	Standard hydrogen electrode
SR	SRP receptor
SRP	Signal recognition particle
T2SS	Type two secretion system
TCEP	Tris(2-carboxyethyl)phosphine
TMBD	N,N,N',N'-Tetramethyl-1,3-butanediamine
UV-Vis	Ultraviolet-Visible

Chapter 1. Introduction

There is little argument that hemes are among the most important co-factors in biology. Some of the most well studied proteins in history contain heme prosthetic groups, which are often noted to be key to function and are at the centre of interest and study of these proteins. Hemoglobin and myoglobin, critical proteins concerning gas transport and storage throughout mammalian cardiovascular systems, contain heme cofactors that serve as reversible binding sites for gases (1). Cytochrome *c*, known for its role in respiration and cell apoptosis, has a heme cofactor that is almost completely dominant in the structure of this small protein (2-4). In cytochrome P450, an important enzyme that plays a key role in the catalysis of xenobiotics, the active site is a heme cofactor which incorporates molecular oxygen directly into the carbon chain of insoluble or amphipathic molecules (5). More recently large numbers of gas sensing hemoproteins have been discovered, acting as regulators, and driving responses to fluctuating levels of gases like oxygen and carbon monoxide (6). Hemes also play a central role in the mitochondrial respiration chain, and study of this pathway offers a wealth of knowledge regarding heme mediated electron and ion transport (3).

Electron transport cytochromes have recently become the subject of great interest due to their essential contribution to the respiratory pathways of electrogenic bacteria. These organisms produce electrons via respiration and use electron transport cytochromes to shuttle them across their outer membranes and into the extracellular environment. There are many theorised biotechnological applications for these microorganisms, such as harvesting electrons in microbial fuel cells or energising these electrons to use in renewable chemical synthesis. A model organism for such systems is *Shewanella oneidensis* MR-1 of the family *Shewanellacae*, accepted as a model organism due to its ease of culture and receptiveness to important techniques in microbiology. Although these extracellular cytochromes have been harbouring interest for many years, it was only recently that the mechanisms of electron transport throughout them had been described. In 2021 van Wonderan *et al.* published their findings from an investigation into the mechanisms of electron transport through the electron transport cytochrome MtrC of *S. oneidensis* MR-1 (7). During this investigation the substitution of a histidine ligand to a heme directly impacted its function, changing its spectroscopic properties and increasing its affinity for electrons. These findings sparked the idea to develop a suite of variant MtrC proteins that have had various histidine ligands substituted with possible alternative ligating residues, resulting in hemes throughout the structure having unique spectroscopic features to one another and varying affinity for electrons. Chapter 1 of this thesis aims to briefly introduce the model organism *Shewanella* and the proteins involved in its extracellular electron transport pathway. Following on from this a detailed description of the synthesis and secretion of the protein of interest MtrC is offered, along with the key structural elements that are exploited in experiments throughout this thesis. Finally, the aims and objectives of this work are presented.

1.1 *Shewanella oneidensis* MR-1 and its metal reducing pathway

Shewanella oneidensis MR-1 (formerly *Alteromonas putrefaciens* MR-1) was first noted for its metal reducing properties in 1988 by Myers and Nealson, who isolated the bacteria from lake Oneida, New York state (8). Here they confirmed the hypothesis that such organisms could respire anaerobically using external redox partners such as Fe(III) and Mn(IV) oxyhydroxide particles (8, 9). The *Shewanella* genus was fully described in 1999 by Venkateswaran *et al.* (10), shortly followed by the full genome sequencing of *S. oneidensis* MR-1 a few years later in 2002 (11), becoming a model organism of dissimilatory metal reducing bacteria around the same time. The metal reducing ability of *S. oneidensis* MR-1 is attributed to a collection of hemoproteins that form an electron transport

chain, facilitating electron movement from the cytoplasmic membrane, across the periplasm and outer membrane, into the cell milieu (**Figure 1**) (12).

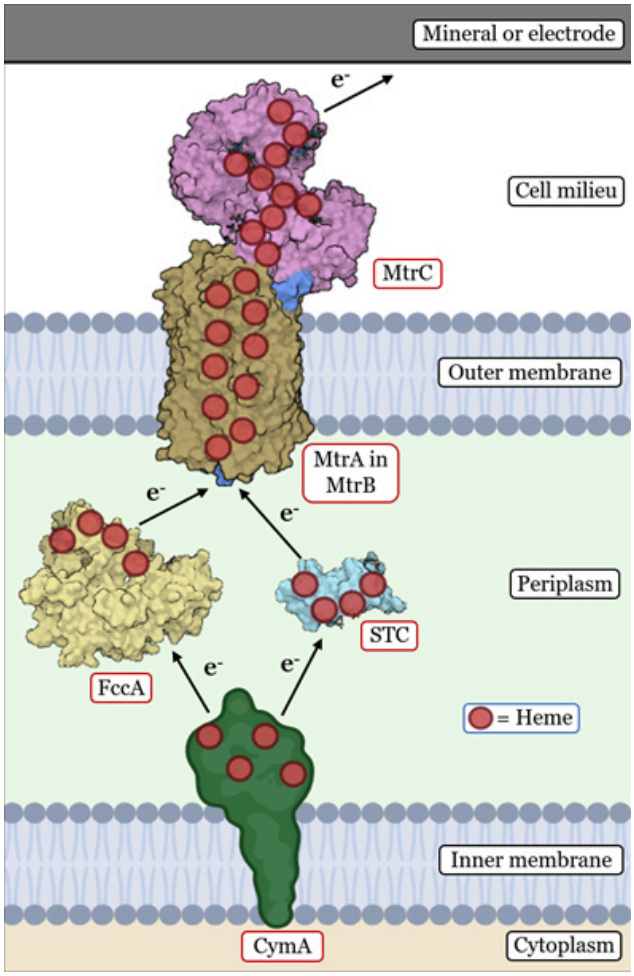

Figure 1. A diagram showing the key proteins involved in the extracellular electron transport pathway of *Shewanella oneidensis* MR-1. All proteins representations based on Protein Data Bank structures from *Shewanella* other than CymA, which has not been structurally resolved in *Shewanella* and is a cartoon representation of an AlphaFold model. PDB codes for FccA: 1QJD, STC: 6EE7, MtrCAB: 6R2Q. A heme cofactor is represented as a red circle.

During anaerobic respiration electrons produced in the inner membrane are shuttled to the quinone oxidoreductase CymA (13). This inner membrane monotopic tetraheme cytochrome has one cofactor binding site specific to menaquinone-7, and a quinone/quinol conversion site (13, 14). Menaquinol-7 oxidation is coupled to the reduction of one of two periplasmic electron carrier proteins, the small tetraheme cytochrome (STC) or the fumarate reductase flavocytochrome c (FccA). Both STC and FccA are shown to interact with the redox partners CymA and MtrA (15-17). STC and FccA are capable of shuttling electrons across the periplasm where they can be received by MtrA of the heterotrimeric electron transport complex MtrCAB (15, 18-20). MtrA sits inside the twenty-six strand β-barrel porin MtrB and is sheltered from the hydrophobic lipid bilayer (21). MtrA contains ten *c*-type hemes in close enough proximity to allow electron transfer across the length of the protein (22). MtrC associates to MtrB and sits externally, facilitating electron transfer to the extracellular environment (23, 24). MtrC contains ten *c*-type hemes that can transfer electrons directly to external minerals, as well as reducing electron shuttles such as flavin mononucleotides (25). Although these proteins have

their own reasons to be the subject of study, this thesis focuses on MtrC. This protein has been the subject of intense study due to its ease of purification, general stability, and the nature of its position as the interface between the electron transport pathway of the cell and the extracellular environment.

1.2 MtrC: Structure, synthesis, and secretion

MtrC is an outer membrane associated electron transport cytochrome composed of four domains - two seven-strand β-barrel domains (I and III), and two heme containing α-helical domains (II and IV) (**Figure 2A**) (25). Each of the heme-binding α-helical domains contains five *c*-type hemes in close proximity to one another, with porphyrin rings separated by no more than seven Angstroms (25). These ten hemes are covalently bound to the protein via the ubiquitous CXXCH binding motif found in the vast majority of *c*-type cytochromes (**Figure 2B**) (25). This motif covalently binds the heme to the protein via two thioether bonds formed between the vinyl groups of the heme and two cysteine residues. To facilitate this covalent attachment, a histidine residue is ligated to the iron in the proximal position during protein maturation (26). The distal ligand of *c*-type cytochromes can vary, however all hemes in MtrC are distally ligated by a histidine residue, making the heme ligand sets in MtrC all His/His (25). The arrangement of hemes within MtrC assumes a distinctive 'staggered cross' formation that runs through the entire protein structure (25). MtrC is bound to MtrB in such a way as to leave heme five of MtrC within eight Angstroms of heme ten of MtrA (20). This close connection between the hemes of MtrA and MtrC facilitates electron movement from the periplasm to the extracellular environment, although the exact points of electron egress from MtrC are unknown (20).

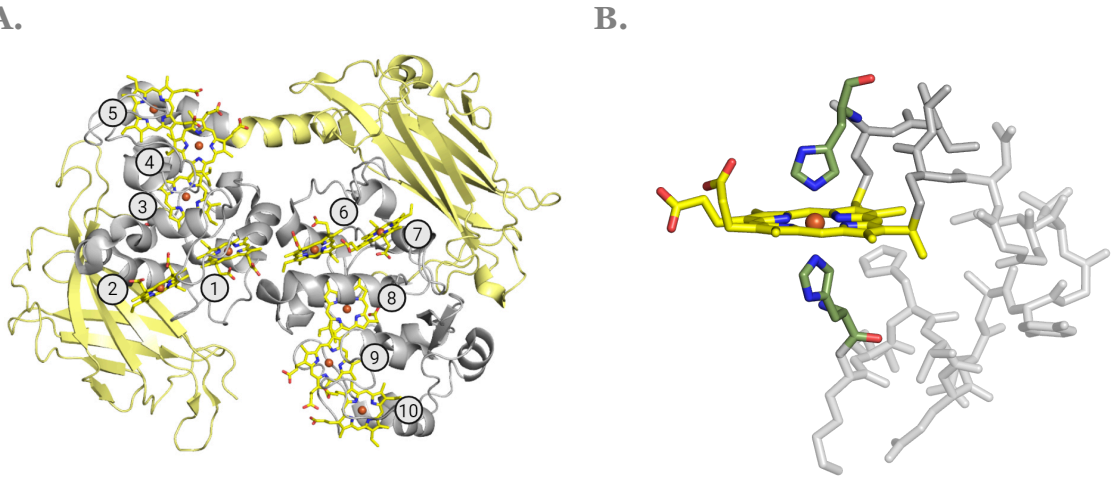

Figure 2. A) The crystal structure of the decaheme electron transport cytochrome MtrC of *S. oneidensis*. The hemes of the heme chain running through the protein are coloured yellow and labelled one to ten. The β-barrel domains I and III are pale yellow while the heme containing domains II and IV are grey. **B)** The CXXCH binding motif of heme eight in MtrC. Two cysteine residues of the protein (separated by two amino acids) form thiolate bonds with two vinyl groups of the heme. The proximal histidine of the CXXCH motif can be seen ligating the iron centre of the heme above the distal histidine ligand, separated from the CXXCH motif by any number of amino acids.

MtrC in its wildtype form ($MtrC_{WT}$) is an outer membrane bound lipoprotein, with a post translational N-terminal lipid anchor modification (27). Recombinant soluble MtrC ($MtrC_{Sol}$) is routinely purified via affinity chromatography, with this lipid modification absent from the final folded protein (28). A comparison of the gene sequences for $MtrC_{WT}$ and $MtrC_{Sol}$ (**Figure 3**) shows the only modifications are

at the N- and C-terminus of the protein (28). In order to understand why and how these two variations of the same protein are different, and what role the gene modifications play in it, the pathway that MtrC takes from synthesis in the ribosome to secretion to the cell milieu must be considered. Bacterial secretion of proteins is generally well studied due to its importance in many key functions of bacterial survival, and critically, its role in pathogenesis (29). *Shewanella* is no exception to this, and work has previously described the specific pathways that the pathogen *S. putrefaciens* uses for secretion of proteins across its external membrane (29, 30). This coupled with the work done by Shi *et al.* (30) that shows that MtrC and its homologue OmcA use the Type II secretion system, and work done by Kranz *et al.* (31) that shows *S. oneidensis* MR-1 uses the Ccm system to mature its cytochromes, gives a good picture of the pathway this heme containing lipoprotein takes from synthesis to function.

```
MTRC_WT     MMNAQKSKIA LLLAASAVTM ALTGCGGSDG NNGNDGSDGG EPAGSIQTLN     50
MTRC_SOL    MKFKLNLITL ALLANTGLAV AAD  GGSDG NNGNDGSDGG EPAGSIQTLN     48

MTRC_WT     LDITKVSYEN GAPMVTVFAT NEADMPVIGL ANLEIKKALQ LIPEGATGPG     100
MTRC_SOL    LDITKVSYEN GAPMVTVFAT NEADMPVIGL ANLEIKKALQ LIPEGATGPG     98

MTRC_WT     NSANWQGLGS SKSYVDNKNG SYTFKFDAFD SNKVFNAQLT QRFNVVSAAG     150
MTRC_SOL    NSANWQGLGS SKSYVDNKNG SYTFKFDAFD SNKVFNAQLT QRFNVVSAAG     148

MTRC_WT     KLADGTTVPV AEMVEDFDGQ GNAPQYTKNI VSHEVCASCH VEGEKIYHQA     200
MTRC_SOL    KLADGTTVPV AEMVEDFDGQ GNAPQYTKNI VSHEVCASCH VEGEKIYHQA     198

MTRC_WT     TEVETCISCH TQEFADGRGK PHVAFSHLIH NVHNANKAWG KDNKIPTVAQ     250
MTRC_SOL    TEVETCISCH TQEFADGRGK PHVAFSHLIH NVHNANKAWG KDNKIPTVAQ     248

MTRC_WT     NIVQDNCQVC HVESDMLTEA KNWSRIPTME VCSSCHVDID FAAGKGHSQQ     300
MTRC_SOL    NIVQDNCQVC HVESDMLTEA KNWSRIPTME VCSSCHVDID FAAGKGHSQQ     298

MTRC_WT     LDNSNCIACH NSDWTAELHT AKTTATKNLI NQYGIETTST INTETKAATI     350
MTRC_SOL    LDNSNCIACH NSDWTAELHT AKTTATKNLI NQYGIETTST INTETKAATI     348

MTRC_WT     SVQVVDANGT AVDLKTILPK VQRLEIITNV GPNNATLGYS GKDSIFAIKN     400
MTRC_SOL    SVQVVDANGT AVDLKTILPK VQRLEIITNV GPNNATLGYS GKDSIFAIKN     398

MTRC_WT     GALDPKATIN DAGKLVYTTT KDLKLGQNGA DSDTAFSFVG WSMCSSEGKF     450
MTRC_SOL    GALDPKATIN DAGKLVYTTT KDLKLGQNGA DSDTAFSFVG WSMCSSEGKF     448

MTRC_WT     VDCADPAFDG VDVTKYTGMK ADLAFATLSG KAPSTRHVDS VNMTACANCH     500
MTRC_SOL    VDCADPAFDG VDVTKYTGMK ADLAFATLSG KAPSTRHVDS VNMTACANCH     498

MTRC_WT     TAEFEIHKGK QHAGFVMTEQ LSHTQDANGK AIVGLDACVT CHTPDGTYSF     550
MTRC_SOL    TAEFEIHKGK QHAGFVMTEQ LSHTQDANGK AIVGLDACVT CHTPDGTYSF     548

MTRC_WT     ANRGALELKL HKKHVEDAYG LIGGNCASCH SDFNLESFKK KGALNTAAAA     600
MTRC_SOL    ANRGALELKL HKKHVEDAYG LIGGNCASCH SDFNLESFKK KGALNTAAAA     598

MTRC_WT     DKTGLYSTPI TATCTTCHTV GSQYMVHTKE TLESFGAVVD GTKDDATSAA     650
MTRC_SOL    DKTGLYSTPI TATCTTCHTV GSQYMVHTKE TLESFGAVVD GTKDDATSAA     648

MTRC_WT     QSETCFYCHT PTVADHTKVK M                                    671
MTRC_SOL    QSETCFYCHT PTVADHTKVK MSAWSHPQFE K                         679
```

Figure 3. A comparison of the gene sequences of $MtrC_{WT}$ and $MtrC_{Sol}$, with the differences in the sequence highlighted in red. Differences at the N-terminus are where the signal sequence of $MtrC_{WT}$ has been replaced that of MtrB (28). C-terminal changes are the addition of a StrepII tag to aid in affinity chromatography during protein purification (28).

Synthesis of MtrC occurs in the ribosome, and from here a small section of peptide at the N-terminus of the protein will dictate the path that the nascent protein chain takes from the ribosome to the

cytoplasmic membrane transporter. N-terminal signal peptide sequences are ubiquitous in proteins that require secretion across membranes in both prokaryotes and eukaryotes (32). These short peptide sequences (typically 25-30 residues in prokaryotes) are composed of three main segments, the positive N-terminal region, the hydrophobic α-helical core, and the C-terminal cleavage site (32). There are two general secretory pathways for protein translocation across the cytoplasmic membrane in prokaryotes, the Sec and Tat dependent pathways (33). Sec and Tat signal peptides differ in a number of ways, and these differences are enough that computational software such as SignalP6.0 can identify their differences and predict the pathway a protein will follow (34). Analysis of the signal peptide of $MtrC_{WT}$ determines that the protein uses the Sec-dependent general secretory pathway for translocation across the cytoplasmic membrane and into the periplasm (34, 35). However, the analysis of the signal peptide gives no insight into the method of transport the protein utilises to get from the ribosome to the SecYEG translocon, and it has not yet been described experimentally. Three potential paths can be utilised here which are detailed in **Figure 4.** The first method is a co-

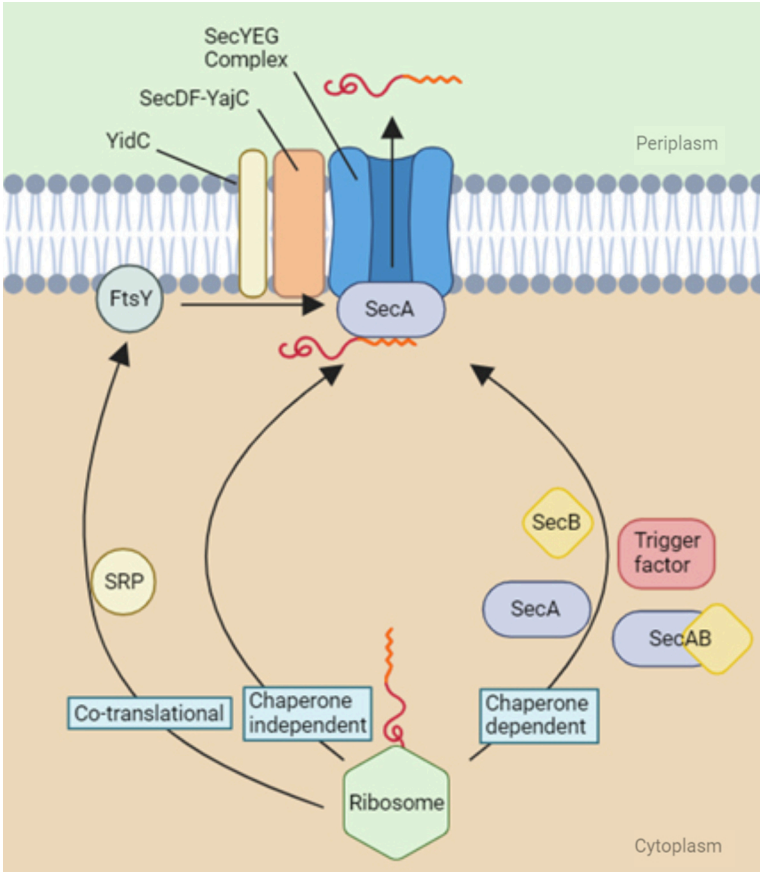

Figure 4. The pathway MtrC will take from synthesis in the ribosome to the periplasm. The nascent protein chain (red) shown with its hydrophobic signal helix (orange) emerging from the ribosome. At this point the protein chain will take 1 of 3 pathways. 1) Co-translational transport involves binding with the Signal Recognition particle (SRP) followed by the bacterial SRP Receptor (SR) before being translocated across the SecYEG complex. 2) Chaperone independent transport has the protein chain find its way across the cytoplasm independently before binding to the SecA-SecYEG complex. 3) Chaperone dependent transport is mediated by a host of potential chaperone proteins including SecA, SecB, SecAB, or trigger factor. Regardless of whether the protein was chaperoned or independently found its way to the membrane, it is bound to the ATPase motor SecA to assist in transport through SecYEG. SecDF-YajC and YidC have been shown to increase translocation efficiency.

translational step involving the ribonucleoprotein Signal Recognition Particle (SRP) and the bacterial SRP Receptor (SR) FtsY (35, 36). The ribosome bound SRP recognises the N-terminal protein signal sequence as it is emerging from the ribosome and targets the complex to the SecYEG translocon via interaction with the SR FtsY (36). Here the protein chain is translocated directly across the cytoplasmic membrane and into the periplasm. Post-translational translocation of the nascent protein chain can be either mediated by a chaperone (SecA, SecB, SecAB, or trigger factor) or simply left to diffuse alone and bind to SecA, an essential and conserved translocase adenosine triphosphate (ATP) driven motor in bacteria (35). SecA will either be SecYEG-bound or freely diffusing in the cytoplasm (35). Once bound, the nascent protein chain-SecA complex binds to SecYEG and SecYEG-A mediates transport of the chain across the cytoplasmic membrane (35). SecDF-YajC and YidC have been shown to increase translocation efficiency (35). *S. oneidensis* MR-1 carries the gene for all proteins discussed in this section (NCBI genome assembly GCF_000146165.2). However, it is understood that no literature is available describing which pathway MtrC takes from synthesis in the ribosome to the SecYEG translocon.

Once in the periplasm covalent attachment of *b*-type hemes into the unfolded peptide chain can occur. For heme incorporation into the peptide chain *b*-type hemes must be translocated from the site of synthesis in the cytoplasm to the periplasm. The exact mechanism of this translocation is unclear, however the involvement of CcmABCD and CcmE appears essential and selective to *c*-type cytochromes (31). CcmC is thought to receive the *b*-type heme and store it in a conserved tryptophan rich region (WWD) in its chain (26). CcmA subunits are ATPases and CcmB and CcmD span the membrane. A general outline of the steps involved in *b*-type heme transport across the cytoplasmic membrane and incorporation into the unfolded protein chain is shown in **Figure 5.**

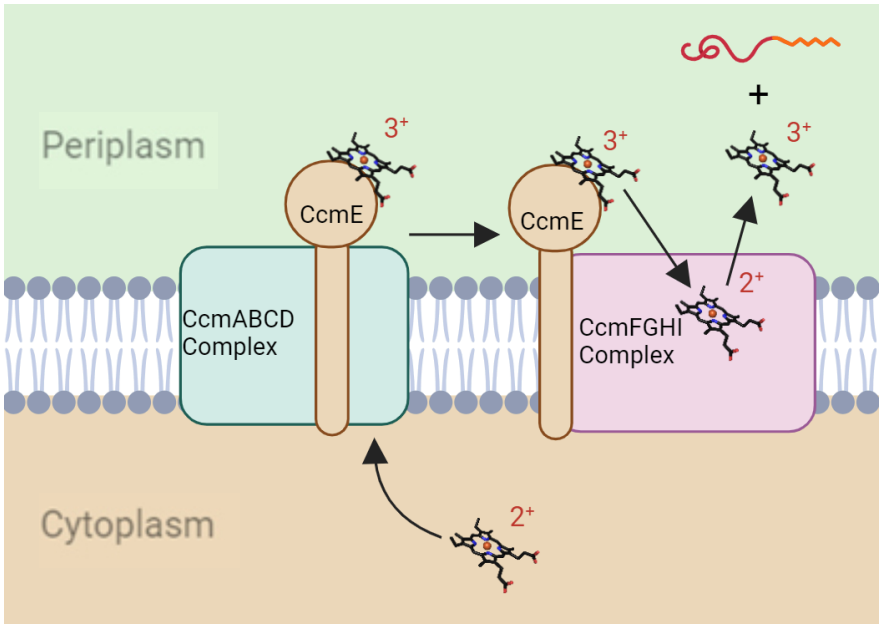

Figure 5. An overview of the path a *b*-type heme takes from cytoplasm to periplasm. The *b*-type heme binds to a trypotophan rich region of the cytoplasmic membrane associated CcmC. Here CcmE binds the *b*-type heme, dissociates from CcmABCD and moves across the cytoplasmic membrane. It binds to CcmFGHI where the heme is subsequently folded into the nacesnt protein chain (red and orange). The oxidation state of the iron in the *b*-type heme throught this process is shown in red.

Covalent attachment of the *b*-type hemes in MtrC is achieved through thioether linkages from the cysteines of the protein CXXCH motif to two peripheral vinyl groups in the *b*-type heme porphyrin ring, a mechanism for which is shown in **Figure 6.** The proximal histidine ligand from the CXXCH motif also plays an important role in heme incorporation, where it ligates the iron centre early in the process. The mechanism detailing electron transfer in this system is debated and complex, and consequently not discussed further in this thesis.

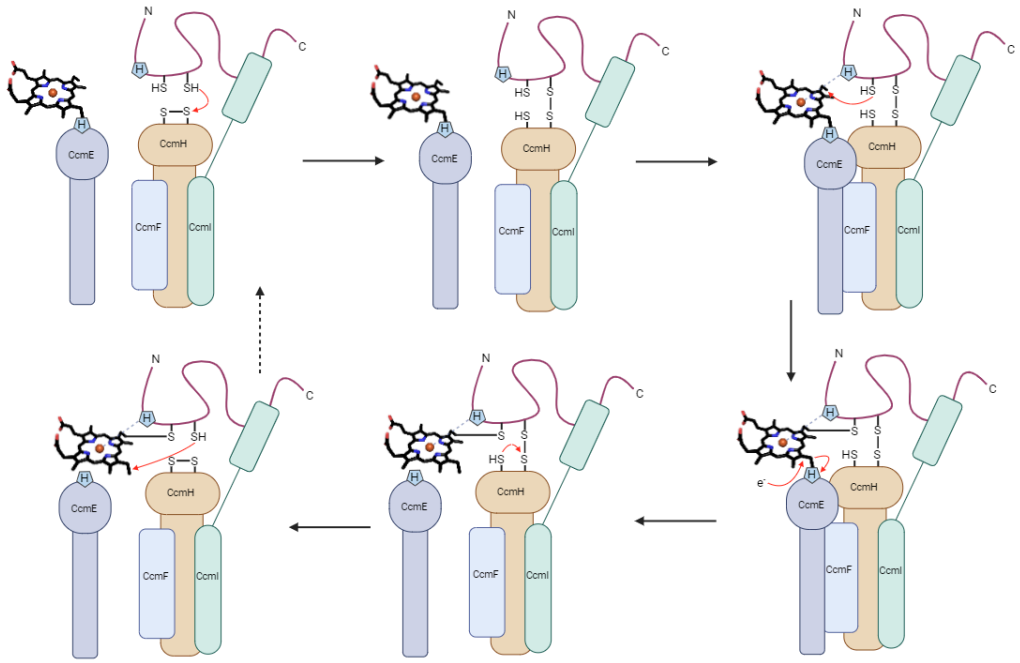

Figure 6. The Ccm system for cytochrome maturation. The *b*-type heme is transported by the holoenzyme CcmE from the CcmABCD complex to CcmFGHI. CcmG is excluded from this figure due to its lack of direct involvement in this mechanism. CcmE is regenerated in the second to end step and can re-ligate to CcmABCD, ready to complete another cycle.

At this stage the matured MtrC is folded with a full roster of ten *c*-type hemes, and still retains the signal peptide at the N-terminus. In $MtrC_{WT}$ the signal peptide contains a 'lipobox', a conserved sequence of amino acids at the C-terminus of the signal peptide (**Figure 3**). A cysteine at position +1 of the lipobox is the site of fatty acid attachment in the protein and the new N-terminus when the remaining signal peptide is cleaved at later stages in the maturation process (37). The signal peptide is recognised first by the protein diacylglyceryl transferase Lgt which performs post-translational lipid modification by catalysing the addition of a diacylglyceryl to the conserved cysteine residue in the lipobox of the protein signal peptide (37). This releases a small molecule, for example glycerol-1-phosphate, and prepares the protein for signal peptide cleavage by LspA (37). Once the signal peptide is cleaved the protein is targeted for transport through the periplasm and across the outer membrane. Here a key difference between $MtrC_{WT}$ and $MtrC_{Sol}$ is seen, as $MtrC_{Sol}$ does not have the same N-terminal signal sequence as its wildtype counterpart (**Figure 3**). The N-terminal signal sequence of $MtrC_{Sol}$ has been replaced with that of MtrB (28). This replacement ensures the protein is targeted for maturation and secretion in the same way as $MtrC_{WT}$ but does not contain a lipobox motif. This results in $MtrC_{Sol}$ being matured as a *c*-type cytochrome without the lipid anchor, forming a soluble version of the protein.

Translocation of MtrC across the outer membrane must now occur, and this is achieved by the type II secretory system (**Figure 7**) (30). The type II secretory system (T2SS) is a double membrane spanning protein complex composed of between twelve and fifteen components, many of which are proteins that form large multimeric structures containing upwards of ten subunits (33). These proteins are named general secretion pathway proteins (Gsp proteins) and can be grouped into four main categories, the cytoplasmic ATPase GspE, the cytoplasmic membrane platform proteins GspCFLM, the periplasmic pseudolipids GspGHIJK, and finally the periplasmic membrane channel GspD. Individual proteins in this system are generally well understood but how the mechanism as a whole functions is not yet described. It is understood that the fully folded protein destined for the cell milieu or periplasmic membrane is recruited by GspC and the ATP hydrolysing activity of GspE causes a rotary system to pump the protein through the periplasmic pseudolipid structure and across the periplasmic membrane via the membrane channel GspD (33). Here $MtrC_{WT}$ will be membrane bound via its lipid anchor and will associate to MtrAB where it can begin functioning as a fully matured electron transport cytochrome. In contrast, $MtrC_{Sol}$ does not contain the lipid anchor and will consequently be excreted into the cell milieu. Here, $MtrC_{Sol}$ can be purified using the C-terminal modification of a StrepII tag (28). This StrepII tag has high affinity for a StrepTactin purification column, and can be separated from the spent media in a one step purification process (28). These two N- and C-terminal modifications to MtrC have been shown to have no effect on the tertiary structure or the functionality of the mature protein (28).

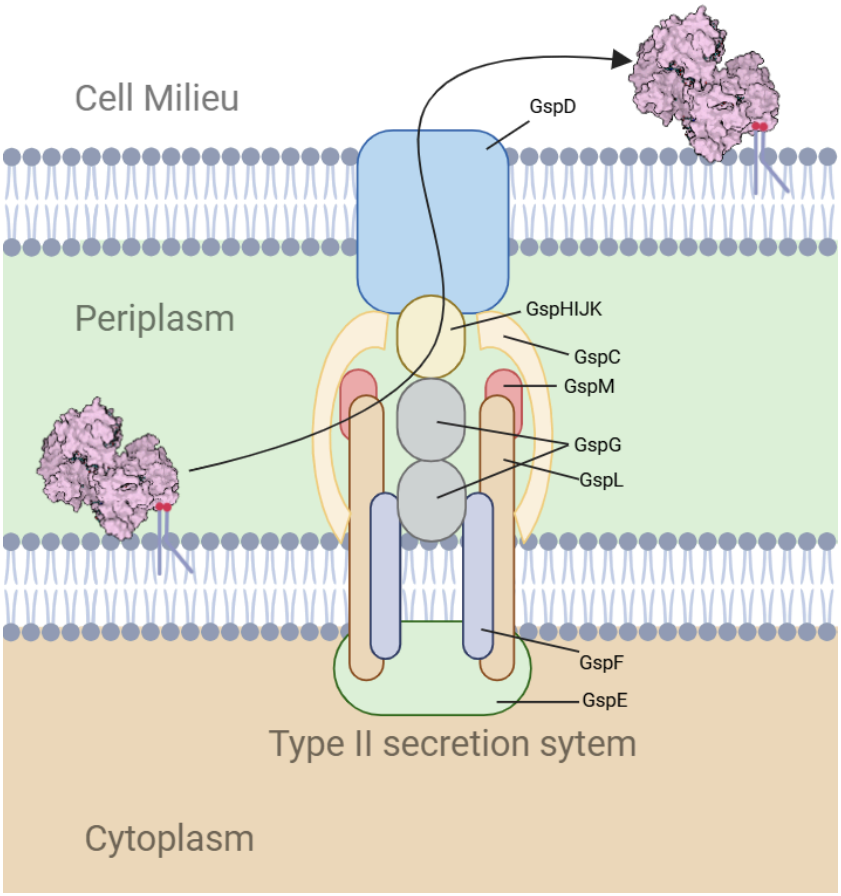

Figure 7. A predicted structure of the T2SS complex. MtrC (pink) with its lipid anchor can be seen entering via GspC and being forced upwards through the pumping of GspG monomers into the pseudolipid chamber below.

1.3 Heme ligation and electron transfer in MtrC

Heme is a planar yet highly asymmetric molecule. While there are twelve possible stereoisomers of protoheme, only isomer IX (protoporphyrin IX) is found in biological systems and serves as the precursor to all heme groups. The core structure is an aromatic porphyrin macrocycle composed of four pyrrole subunits linked together by methine (-CH=) bridges (**Figure 8**). Protruding from the porphyrin macrocycle are various substituent groups that vary depending on the specific heme species, but commonly consist of methyl ($-CH_3$), vinyl ($-CH=CH_2$), and propionic acid ($-CH_2-CH_2-COOH$) side chains. These substituents influence the solubility, reactivity, and protein interactions of the heme prosthetic group. Each pyrrole subunit contains one nitrogen atom coordinated to a central iron atom in a square planar arrangement along the x and y axes. The introduction of axial ligands on the z plane lifts this planar chelation, forming a final octahedral coordination structure around the iron centre.

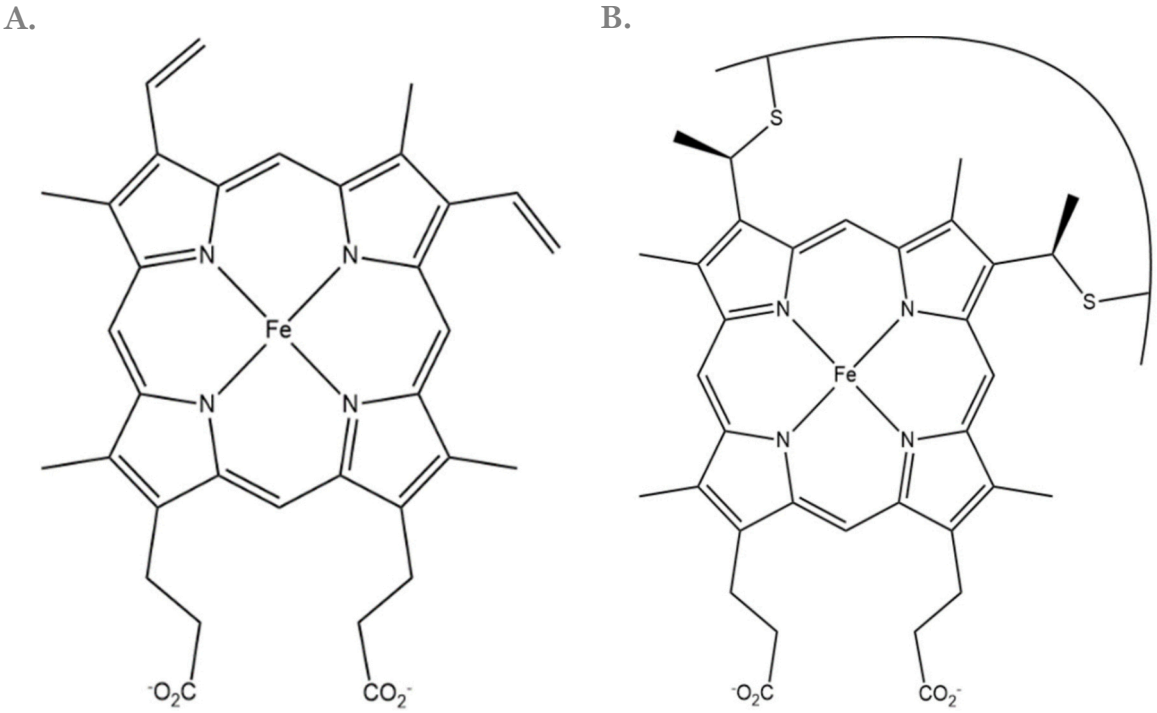

Figure 8. A) The structure of a *b*-type heme compared to **B)** a *c*-type heme. Structurally these two types of heme are similar, with the only differences being a *c*-type heme contains covalent bonds to the protein via two thioether linkages between the heme vinyl groups and two cysteine resides of the CXXCH binding motif in the protein.

Axial heme ligands are diverse; producing an exhaustive list of potential ligands would be a challenging endeavour (38). However, a few common ligands are observed, and the ligand type often hints at the specific function of the hemoprotein (39). The axial ligand is commonly an amino acid side chain such as histidine, methionine, lysine, arginine, or cysteine. Alternatively, it could be an exogenous molecule like water/hydroxide, cyanide, oxygen, or in some cases, the site may remain unligated. The *c*-type hemoproteins are the most restricted in terms of potential ligand sets, as the proximal ligand is typically a histidine residue that plays an essential role in protein maturation. Other amino acid side chains have been observed as proximal ligands to *c*-type hemes (namely lysine in nitrite reductase, NfrA), although this is rare and consequently not acknowledged further in this thesis (40).

MtrC contains ten hemes all covalently bound via the CXXCH binding motif and are axially coordinated by two histidine residues (25). Although all hemes in MtrC are bound by two histidine residues, the redox potential window that these hemes operate in differ substantially, spanning a range of 300 mV (41). These differences in redox potentials between hemes are proposed to be the driving force behind electron transfer throughout these cytochromes. The Moser-Dutton ruler offers estimates of electron transfer rates across biological macromolecules based on the distance between two redox centres and the driving forces of the reaction. In practice, the Moser-Dutton ruler has an effective range of around 8-20 Å between redox centres, representative of the limits at which terms within the equation become negligible. Generally, the Moser-Dutton ruler is applied between redox centres separated by amino acid residues, water, or some other medium. It is not known if the Moser-Dutton ruler would still be an effective predicter of electron transfer rates between hemes in multiheme cytochromes due to these redox centres being in such close proximity (<4-8 Å) and with no other medium separating them.

In 2019 van Wonderen *et al.* detailed the rates of electron transfer within the multiheme cytochrome STC (42). This paper was the first to offer insights into the dynamics of electron transfer within multiheme cytochromes, and it was achieved through light driven electron injection via photosensitisation with a Ru(II)bipyridine$_3$ dye (**Figure 9**).This same technique was later used to describe not only the heme-heme electron transfer dynamics of MtrC, but also give direct evidence for electron transfer across the heme wire, which was up to this point lacking. Evidence of heme-heme transfer along the heme wire of both STC & MtrC is difficult to attain due to there being no spectroscopically distinguishable heme present. This was overcome in MtrC through substitution of the distal ligand of heme eight, a histidine at position 561, to a methionine. This changed the spectroscopic footprint of the heme and allowed for empirical evidence that electrons injected at one end of the heme wire were making it to heme eight and reducing the iron centre. Although not the objective of this methionine substitution, it was noted that this had the effect of creating a high potential centre and electron sink. This His/Met ligated heme increased the lifetime of the charge separated state to the scale of 100 μs from 1 μs (7).

1.4 Aims of the project

When oxidised MtrC is site-selectively labelled with Ru(II)bipyridine$_3$ dye as a photosensitiser (Ru-MtrC), excitation into the dye metal to ligand charge transfer band creates a photoenergised electron that can inject into the heme wire of Ru-MtrC (7). In the presence of Ethylenediaminetetraacetic acid (EDTA) as a sacrificial electron donor, these photoenergised electrons become trapped within the heme wire upon irradiation of Ru-MtrC (**Figure 9B**)(43). This mechanism presents opportunities to utilise Ru-MtrC as a light-driven redox catalyst (**Figure 9C**). However, for efficient conversion of energy (photons) to desired chemical reactions, the residency time of the photoenergised electrons within the heme wire must be increased. In other words, the rate of non-productive electron return to the Ru(II)bipyridine$_3$ dye, which wastes energy, needs to be minimised. Introduction of a high potential centre to MtrC though His/Met ligation of a heme increases the time photoexcited electrons spend in the heme wire, a favourable feature when considering reaction dynamics with a catalyst.

Consider the opposite, MtrC with ten hemes in the reduced Fe(II) form, and a surface mounted dye that when photoexcited removes an electron from the heme wire, another viable pathway to favourable photocatalytic reactions. This photooxidation could, in theory, be stabilised with the

introduction of a low potential centre in the heme wire, proposed to be achievable via a cysteine distal ligand to a heme. Examples in biology follow the trend of cysteine ligated hemes having low redox potentials, including cytochrome P450 and SoxAX. Cytochrome P450, a *b*-type cytochrome with cys/water ligation is reported to have a resting potential of below -300 mV to prevent auto reduction (44). SoxAX is a sulfur oxidising enzyme that contains three hemes, one of which is a *c*-type heme ligated by a proximal histidine and a distal cysteine thiolate residue. This heme in SoxAX has a very low resting potential of below -400 mV (45, 46). A doctoral thesis from Jenner details modifications to a heme of thiosulfate dehydrogenase (TsdA) from *Campylobacter jejuni* (47). In this thesis Jenner substitutes the distal ligating residues and reports changes to the reduction potentials in line with

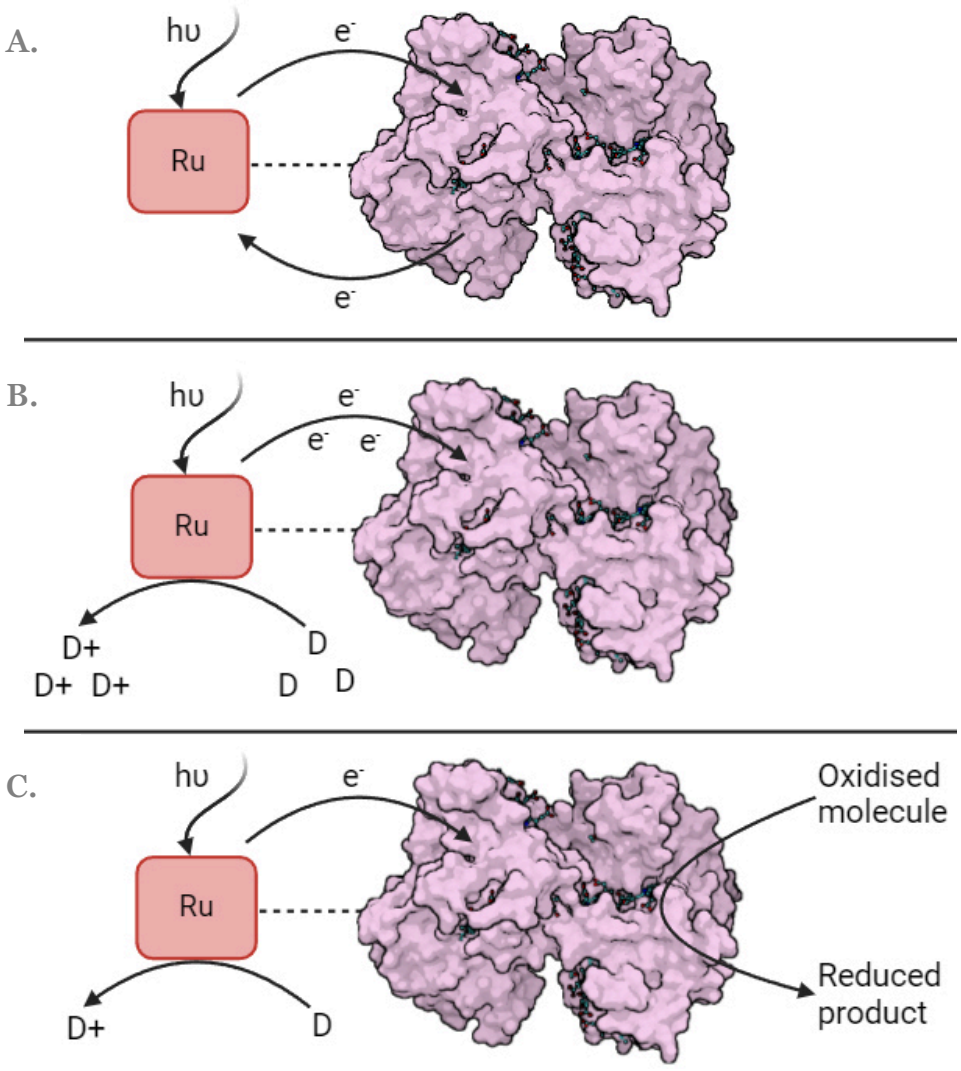

Figure 9. A) A schematic for a photosensitised MtrC with a Ru(II)bipyridine$_3$ dye. Light is exciting an electron in the Ru(II)bipyridine$_3$ dye and it is being injected into the heme wire of MtrC. Charge recombination occurs and the electron comes to rest back on the Ru(II)bipyridine$_3$ dye. **B)** A sacrificial electron donor molecule reducing the Ru(II)bipyridine$_3$ dye as it injects an electron into the heme wire of MtrC. Charge recombination does not occur and MtrC becomes fully reduced with ten electrons. **C)** A sacrificial electron donor molecule reduces the Ru(II)bipyridine$_3$ dye as it injects excited electrons into the heme wire of MtrC. MtrC uses this excited electron and reduces a molecule, creating a regenerating photocatalyst.

what is predicted here (47). These values presented alongside the examples of cytochrome P450 and SoxAX explain the rationale behind the chosen residues for substitution in the MtrC protein, leading on to the primary objective this thesis aims to meet - Produce a suite of variant MtrC proteins with distal histidine heme ligand substitutions to methionine or cysteine, and measure the effects on protein expression, structure, ligand sets, and redox potentials.

The target hemes for distal histidine ligand substitutions in this thesis have been considered carefully. Although not published in the original report by van Wonderen *et al.* (7) multiple sites throughout the MtrC protein were tried as targets of His/Met substitution, with heme eight (H561M) providing a fully folded protein with all low spin heme. For this reason, position H561 will be a target for substitution to a cysteine residue (H561C).

The structure of MtrC shows that the two heme containing domains (II and IV) have high levels of homology. Heme eight is in domain IV, suggesting a good target for substitution will be the distal histidine ligand to heme three, the domain II analogue of heme eight. The distal ligand of heme three is histidine at position 230. It is understood that no substitutions have been attempted to heme three in MtrC, so this project aimed to introduce both methionine (H230M) and cysteine (H230C) substitutions into MtrC.

It should be noted that all proteins produced in this work will also contain a surface tyrosine to cysteine substitution (Y657C). This substitution allows site selective attachment of the Ru(II)bipyridine$_3$ dye to the thiol of cysteine. This substitution lies within the CXXCH binding motif of heme ten, creating a CXCCH motif. It has been shown that this substitution has no discernible impact on protein fold, spectroscopic properties, or redox potential (7). However, X-ray crystallographic structural refinement of a protein containing this substitution has proved impossible, as introducing this surface cysteine residue impacts formation of protein crystals. Since this represents such a critical gap in knowledge surrounding this subject, a short investigation into determining the structure of the Y657C substitution is made.

Chapter 2. Materials and Methods

2.1 Plasmid mutagenesis

Plasmids pBAD.C_{Sol}^{Y657C} and pBAD.$C_{Sol}^{Y657C\ H561M}$ were recovered from -20°C storage and thawed on the benchtop (7). Two 50 µL aliquots of TOP10 competent cells (Thermo Fisher) were recovered from lab stock -80°C storage, thawed on the benchtop, and left to incubate on ice for thirty minutes with 3 ng/µL of either pBAD.C_{Sol}^{Y657C} or pBAD.$C_{Sol}^{Y657C\ H561M}$ plasmids. The cells were heat shocked at 42°C for ninety seconds before being returned to ice for a further five minutes. Each sample then had 0.5 mL of S.O.C medium (Thermo Fisher) added, and the cells were allowed to recover for forty-five minutes in a 37°C shaking incubator, 180 rpm. After recovery, the cells were spread on LB plates with 30 µg/mL kanamycin and left to grow overnight in a 37°C incubator. Single colonies were picked from these plates and used to inoculate 10 mL of LB with 30 µg/mL kanamycin, which were then left to grow overnight in a 37°C shaking incubator, 180 rpm. Plasmids were purified according to the GenElute Plasmid Miniprep Kit (Sigma-Aldrich), with molecular grade water being used in the final elution step. Plasmids were prepared for sequencing according to the Mix2Seq Kit (Eurofins Genomics) using the sequencing primers listed in **Table 1.** Sanger sequencing of the plasmids was performed by Eurofins Genomics.

Table 1. *List of mutagenic and sequencing primers. Only the mutagenic primers that resulted in successful incorporation of the desired mutations are shown. Mutagenic primers have their mutations underlined and in bold.*

	Primer	Primer Sequence 5'-3'	Source
Sequencing	TrxFus For	TTCCTCGACG CTAACCTG	Lab stock
	MtrC1 For	CGTTGTTTCT GCTGCGGG	Lab stock
	MtrC2 For	GTTACACACA GCCAAAACCA C	Lab stock
	MtrC3 For	GTTAACATGA CAGCCTGTGC	Lab stock
	pBAD Rev	CCTGATACAG ATTAAATCAG AA	Lab stock
	MtrC4 Rev	GCCTACGGCC TCATTGGT	Lab stock
	MtrC5 Rev	GAGCTCTTGA TCCAAAAGCT AC	Lab stock
	MtrC6 Rev	GCCAACAAAG CTTGGGGC	Lab stock
Mutagenic	Kr01 For	GGTGCGCTAG AGCTAAAACT A**TGT**AAAAAA CACGTTGAAG ATG	This study
	Kr02 Rev	CATCTTCAAC GTGTTTTTT**A** **CA**TAGTTTTA GCTCTAGCGC ACC	This study
	Introduces a histidine to cysteine mutation into the gene of $MtrC_{Sol}$ at position 561 via a coding triplet change of CAC to TGT.		
	Kr03 For	TTAATT**ATG**A ATGTGCATAA TGCCAACAAA GCTTG	This study
	Kr04 Rev	GCACATT**CAT** AATTAAGTGA CTAAAGGCGA CAT	This study
	Introduces a histidine to methionine mutation into the gene of $MtrC_{Sol}$ at position 230 via a coding triplet change of CAC to ATG.		
	Kr05 For	TTAATT**TGT**A ATGTGCATAA TGCCAACAAA GCTTG	This study
	Kr06 Rev	GCACATT**ACA** AATTAAGTGA CTAAAGGCGA CAT	This study
	Introduces a histidine to cysteine mutation into the gene of $MtrC_{Sol}$ at position 230 via a coding triplet change of CAC to TGT.		

Plasmid pBAD.C_{Sol}^{Y657C} was used as template DNA for PCR, a map of which can be seen in **Figure 10.** Primers used to introduce point mutations into the plasmid are listed in **Table 1.** PCR was performed in accordance with the Thermo Scientific Phusion Flash High-Fidelity PCR Master Mix 2-step PCR protocol. PCR products were digested using Thermo Scientific FastDigest DpnI to remove methylated DNA before being heat treated at 85°C for fifteen minutes to inactivate Dpn1. PCR products were washed to remove unused nucleotides and primers using the GenElute PCR Clean-Up Kit. Plasmids were prepared for sequencing according to the Mix2Seq Kit (Eurofins Genomics) using the sequencing primers listed in **Table 1**. Sanger sequencing of the plasmids was performed by Eurofins Genomics. Once confirmed by sequencing, the plasmids pBAD.$C_{Sol}^{Y657C\ H561C}$, pBAD.$C_{Sol}^{Y657C\ H230M}$, and pBAD.$C_{Sol}^{Y657C\ H230C}$ were cloned in an identical way to pBAD.C_{Sol}^{Y657C} and pBAD.$C_{Sol}^{Y657C\ H561M}$ in the first paragraph of this section. Cells were prepared for long term storage by inoculating 10 mL of LB with 30 µg/ml kanamycin with one colony and leaving overnight in a 37°C shaking incubator, 180 rpm. From the overnight culture, 0.5 mL was mixed thoroughly with 1 mL of sterile 50% glycerol water solution and snap frozen in liquid nitrogen before being stored at -80°C. A complete list of plasmids can be found in **Table 2.**

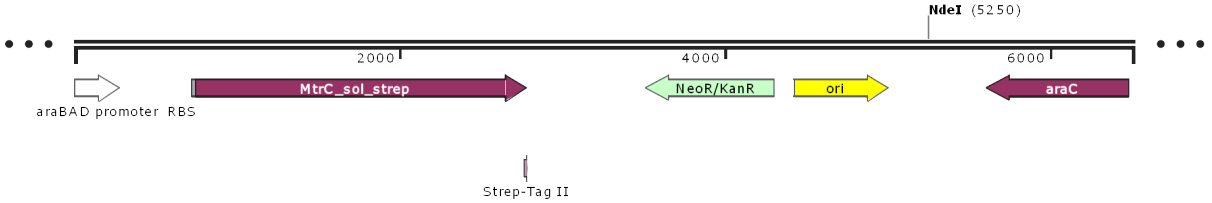

Figure 10. A linear plasmid map of pBAD202. The $MtrC_{Sol}$ gene is under the control of an L-arabinose inducer. The plasmid also confers kanamycin resistance.

2.2 *S. oneidensis* MR-1 electroporation

The following electroporation method was performed for each of the plasmids pBAD.$C_{Sol}^{Y657C\ H561C}$, pBAD.$C_{Sol}^{Y657C\ H230M}$, and pBAD.$C_{Sol}^{Y657C\ H230C}$ to produce a corresponding strain for each. *S. oneidensis* MR-1 cells were sourced from lab stock and used to inoculate 10 mL LB which was left to grow overnight in a 30°C shaking incubator, 180 rpm. From the overnight culture 1.5 mL was centrifuged at 4000 ×g for two minutes in a 1.5 mL Eppendorf tube. The supernatant was removed, and the cell pellet resuspended in 1 mL of 10% glycerol solution and centrifuged again at 4000 ×g for 2 minutes. This wash step was repeated, and the supernatant removed before resuspending the cell pellet in 80 µL of 10% glycerol to bring the total volume up to ~100 µL. From the DNA isolated from *E. coli* (detailed in section 2.1), 3 ng/µL of the relevant plasmid was added, and the cells were electroporated using a BIO-RAD MicroPulser at 1.2 keV. Immediately 0.5 mL of S.O.C medium (Thermo Fisher) was added to the cuvette and mixed before the cells were returned to their Eppendorf tube. The cells were left to recover for three hours in a 30°C shaking incubator, 180 rpm. The cells were finally plated onto LB plates with 30 µg/ml kanamycin and left to grow overnight in a 30°C incubator. Long term storage of cells was made by the method detailed at the end of section 2.1. A complete list of strains and their associated plasmids can be found in **Table 2.**

2.3 Protein expression trials

Four induction conditions were tested by varying the concentration of L-arabinose during cell growth (0 mM, 2 mM, 5 mM, or 10 mM of L-arabinose) as well as two technical replicates of each condition being run in parallel. Eight 100 mL flasks containing M72 media with M72 additions and 30 µg/mL

kanamycin were prepared (recipes for M72 media and M72 additions can be found in the table of abbreviations). A single colony of either MR1.pBAD.$C_{Sol}^{Y657C\ H561C}$, MR1.pBAD.$C_{Sol}^{Y657C\ H230M}$, or MR1.pBAD.$C_{Sol}^{Y657C\ H230C}$ was picked from a plate and used to inoculate a 20 mL flask of LB with 30 µg/ml kanamycin, which was grown overnight in a 30°C shaking incubator, 180 rpm. From this overnight culture 2 mL aliquots were used to perform a 2% inoculation of each 100 mL flask. The flasks had their initial optical density at 600 nm (OD_{600}) recorded using a WPA colourwave CO7500 Colorimeter. The cell growth was then monitored by recording the OD_{600} hourly until it reached between 0.35-0.45, at which point the cultures were induced with between 0-1 mL of 1 M L-arabinose depending on the desired final concentration. Samples continued to have their OD_{600} measured hourly for five more hours before being left overnight in a 30°C shaking incubator, 180 rpm. An additional OD_{600} measurement was taken in the morning of the next day. A sample of each flask was prepared for ultraviolet-visible (UV-Vis) electronic absorbance spectroscopy by centrifuging 1 mL of cell culture at 16,000 ×g for ten minutes and placing the supernatant into a 1 cm quartz cuvette. Electronic absorbance was recorded between wavelengths 300-700 nm using a Cary 60 UV-Vis Spectrophotometer (Agilent). Sodium dodecyl sulfate–polyacrylamide gel electrophoresis (SDS-PAGE) was performed in accordance with section 2.5.

Table 2. *List of plasmids and their associated strains.*

Plasmid name	Relevant features	Associated strain	Source
pBAD.C_{Sol}	A pBAD TOPO derivative that encodes for $MtrC_{Sol}$. This gene is under the control of an L-arabinose inducer. Also confers kanamycin and neomycin resistance.	MR1.pBAD.C_{Sol}	(37)
pBAD.C_{Sol}^{Y657C}	pBAD.C_{Sol} with a surface tyrosine to cysteine mutation at position 657 in the gene of $MtrC_{Sol}$.	MR1.pBAD.C_{Sol}^{Y657C}	(31)
pBAD.$C_{Sol}^{Y657C\ H561M}$	pBAD.C_{Sol} with a surface tyrosine to cysteine mutation at position 657, and a histidine to methionine mutation at position 561 in the coding region of $MtrC_{Sol}$.	MR1.pBAD.$C_{Sol}^{Y657C\ H561M}$	(31)
pBAD.$C_{Sol}^{Y657C\ H561C}$	pBAD.C_{Sol} with a surface tyrosine to cysteine mutation at position 657, and a histidine to cysteine mutation at position 561 in the coding region of $MtrC_{Sol}$.	MR1.pBAD.$C_{Sol}^{Y657C\ H561C}$	This study
pBAD.$C_{Sol}^{Y657C\ H230M}$	pBAD.C_{Sol} with a surface tyrosine to cysteine mutation at position 657, and a histidine to methionine mutation at position 230 in the coding region of $MtrC_{Sol}$.	MR1.pBAD.$C_{Sol}^{Y657C\ H230M}$	This study
pBAD.$C_{Sol}^{Y657C\ H230C}$	pBAD.C_{Sol} with a surface tyrosine to cysteine mutation at position 657, and a histidine to cysteine mutation at position 230 in the coding region of $MtrC_{Sol}$.	MR1.pBAD.$C_{Sol}^{Y657C\ H230M}$	This study

2.4 Protein purification and sample preparation

A single colony of the desired strain was picked from a plate and used to inoculate a 10 mL flask of LB with 30 μg/ml kanamycin which was grown overnight in a 30°C shaking incubator, 180 rpm. From this overnight culture a 2 mL aliquot was used to perform a 2% inoculation of 100 mL of LB with 30 μg/ml kanamycin which in turn was grown overnight in a 30°C shaking incubator, 180 rpm. From this overnight culture two 20 mL aliquots were used to perform a 2% inoculation of two 1 L baffled flasks of M72 Media with M72 additions and 30 μg/ml kanamycin. These flasks then had an OD_{600} measurement taken and were left to grow in a 30°C shaking incubator, 180 rpm. The cell growth was monitored by recording the OD_{600} hourly until the cultures reached between 0.35-0.45, at which point they were each induced with 10 mL of 1 M L-arabinose. The cells were left to grow overnight in a 30°C shaking incubator, 180 rpm. The next morning cells were recovered from the incubator and centrifuged in 1 L canisters in a Beckman Avanti J-20 Centrifuge at 5000 ×g. The spent media was recovered, and the pelleted cells discarded. The protein was separated from the media by affinity chromatography using 2×5 mL StrepTactin columns in series via a GE Healthcare ÄKTA pure (4°C, 5 mL/minute). The StrepTactin columns were washed with 100 mM Tris, 150 mM NaCl, pH 8.1. The protein was eluted using 50 mM Biotin in 100 mM Tris, 150 mM NaCl, pH 8.1, and the columns regenerated using 10 mM NaOH. The protein sample was exchanged into 100 mM Tris, 150 mM NaCl, pH 8.1 and concentrated using 30 kDa spin concentrators at 4500 ×g. SDS-PAGE was performed in accordance with section 2.5.

Once confirmed via SDS-PAGE analysis, the protein sample was purified further via size exclusion chromatography. The protein sample was loop injected onto a Superose 6 Increase 10/300 GL via a GE Healthcare ÄKTA pure (4°C, 3 mL/minute) and fractions were collected in 1.5 mL aliquots. The electronic absorbance at 280 and 410 nm of eluted samples was recorded. Fractions containing material that eluted before or after the main peak based on 410 nm electronic absorbance were discarded. Protein concentrations were estimated using the Beer-Lambert law and known extinction coefficients for $MtrC_{Sol}^{Y657C}$ (7). This was used alongside the 410 nm absorbance of a known dilution of the purified sample which allowed for approximate yields from each purification to be attained by using the volume and estimated concentration of the sample. All protein samples were snap frozen in liquid nitrogen and stored at -80°C.

2.5 Biochemical analysis

For SDS-PAGE analysis, spent media samples (from sections 2.3 and 2.4) or StrepTactin column flowthrough samples (section 2.4) were prepared by mixing the sample with sodium dodecyl sulfate (SDS) loading dye in a 3:1 ratio, and 20 μL of this mixture was loaded into the appropriate lanes. In the case of lanes with purified protein (section 2.4), a mixture of SDS loading dye and 0.66 μM protein was prepared in a 1:1 ratio, and 20 μL of this mixture was loaded into the respective lanes. Samples were boiled at 95°C for fifteen minutes to ensure full denaturation of all material. Each gel had a lane containing 4 μL of BioRad visible protein stain to act as a ladder for molecular weight comparison. Gels containing purified protein (section 2.4) also had a lane containing a previously prepared sample of $MtrC_{Sol}^{Y657C}$ confirmed to be full length via mass spectrometry. BioRad precast gels were submerged in MOPS SDS running buffer, loaded with sample, and set to run at 180 V. All gels were run in duplicate to allow for a Coomassie brilliant blue stain and a heme stain to be applied. Separately the heme stain was performed by washing the gel in reverse osmosis water and leaving it to sit for ten minutes in 25 mL of 0.25 M sodium acetate. While the gel was soaking, 10 mg of

N,N,N',N'-tetramethyl-1,3-butanediamine (TMBD) was dissolved in 10 mL of methanol in a foil covered falcon tube. This was added and left for another ten minutes. To develop the stain 10 µL of 30% hydrogen peroxide was added and the gel was agitated until bands began to develop. The solution was disposed of appropriately, and the gel washed with plenty of reverse osmosis water to prevent over staining. The non-reducing conditions of the SDS-PAGE in these experiments are intentional as reducing conditions interfere with the catalytic heme stain. SDS-PAGE gel images were recorded on a Syngene G:BOX Gel Imaging System.

For liquid chromatography-mass spectrometry (LC-MS), samples of $MtrC_{Sol}^{Y657C\,H561M}$, $MtrC_{Sol}^{Y657C\,H561C}$, and $MtrC_{Sol}^{Y657C\,H230M}$ were treated with tris(2-carboxyethyl)phosphine (TCEP) and left for twenty minutes. Samples were exchanged into a 20 mM Tris, pH 7.0 LC-MS grade ultra performance liquid chromatography (UPLC) water solution to remove excess TCEP, and concentrated to between 20-40 µM protein. A sample volume of 10 µL was loaded onto an ACQUITY UPLC® Protein BEH C4 Column (300 Å, 1.7 µM, 2.1 mm × 50 mm) before being eluted (0.3 mL $minute^{-1}$) using a linear gradient across twenty minutes of increasing acetonitrile (2% to 98%, v/v) in formic acid (0.1% v/v). UPLC was performed by a Waters ACQUITY UPLC H-Class premier. The eluent was ionised via electrospray ionisation at an ionisation energy of 3 kV in positive ion mode. Data was acquired from 500 m/z to 3000 m/z at a scan speed of one second per scan using MassLynx. The system was calibrated with sodium iodide. The data was analysed using UniDec (Universal Deconvolution of Mass Spectra) software.

A set of UV-Vis electronic absorption spectra was produced for each protein $MtrC_{Sol}^{Y657C}$, $MtrC_{Sol}^{Y657C\,H561M}$, $MtrC_{Sol}^{Y657C\,H561C}$, and $MtrC_{Sol}^{Y657C\,H230M}$. All electronic absorbance spectra were recorded between the wavelengths 350-700 nm using a Cary 60 UV-Vis Spectrophotometer (Agilent). The spectrophotometer was baseline subtracted using the spectrum of 100 mM Tris, 150 mM NaCl, pH 8.1 in a quartz cuvette. An aliquot of air equilibrated protein was diluted in a 100 mM Tris, 150 mM NaCl, pH 8.1 until the 410 nm absorbance was ~0.75, and a spectrum was recorded. This sample was fully reduced by titrating in excess sodium dithionite (NaDT) in an anaerobic chamber, sealing the cuvette, and recording a second spectrum. The dilution factor from adding NaDT was accounted for, and a reduced–oxidised difference spectrum was produced.

2.6 Pyridine hemochromagen assay

Due to the volatile and toxic nature of pyridine, and the risk of oxidation from atmospheric oxygen interfering with the experiment, all samples were prepared in an anaerobic chamber and transported in sealed quartz cuvettes. All electronic absorbance spectra were recorded between the wavelengths 350-700 nm using a Cary 60 UV-Vis Spectrophotometer (Agilent). The spectrophotometer was baseline subtracted using the spectrum of a 1 mL aliquot of 100 mM Tris, 150 mM NaCl, pH 8.1 in a quartz cuvette.

The protein sample was diluted in a 100 mM Tris, 150 mM NaCl, pH 8.1 until the absorbance at 410 nm reached ~1.5. From this sample 0.5 mL was mixed with 0.5 mL of 100 mM Tris, 150 mM NaCl, pH 8.1 and a spectrum taken. To this same sample 5 µL of 100 mM potassium ferricyanide ($K_3Fe(CN)_6$) was added to fully oxidise the sample and another spectrum was taken. Comparison of these two spectra via analysis of peak α and β band absorption showed that all samples were fully oxidised at ambient conditions and eliminated the need for an oxidising agent from the rest of this experiment.

A 0.5 mL aliquot of the prepared protein sample was diluted with 0.5 mL of 100 mM Tris, 150 mM NaCl, pH 8.1 and an air oxidised spectrum was taken. This sample was fully reduced by titrating in excess NaDT and a spectrum was taken. The dilution factor from adding NaDT was accounted for, and a reduced–oxidised difference spectrum was produced. These three spectra are hereafter referred to as the 'oxidised', 'reduced', and 'difference' spectra.

A 0.5 mL aliquot of a 200 mM NaOH, 40% (v/v) pyridine solution was mixed with 0.5 mL of the protein sample and a spectrum was taken. To this cuvette 9 µL of NaDT was added and another spectrum was taken. An additional 1 µL of NaDT was added and another spectrum was taken to ensure the sample was fully reduced. Lastly, a spectrum was taken of the same sample one minute later to ensure re-oxidation was not occurring. The dilution factor from adding 10 µL NaDT was factored in only for the NaDT reduced protein samples. A reduced–oxidised difference spectrum was then produced. The absorbance of the difference spectrum at 535 nm was taken from the absorbance at 550 nm. This absorbance was used in the Beer-Lambert equation along with the extinction coefficient for pyridine ligated *c*-type heme (23.97 mM^{-1} cm^{-1}) to get the concentration of pyridine ligated hemes in solution (48). Dividing by ten (the number of *c*-type hemes in $MtrC_{Sol}$) gives the concentration of the $MtrC_{Sol}$ variant in solution. Using this concentration along with the oxidised, reduced, and difference spectra detailed earlier in this section allows for accurate extinction coefficient calculation for each $MtrC_{Sol}$ variant. This assay was repeated to provide five technical replicates so an accurate average value could be produced.

2.7 Magnetic circular dichroism spectroscopy

MCD spectroscopy was performed at room temperature using a JASCO J810 circular dichrograph for wavelengths in range 240 – 850 nm. A magnetic field was generated using a JASCO PM-491 permanent magnet. The magnet was calibrated using MCD of the well studied proteins myoglobin and cytochrome *c* (both from equine heart). Benchmark intensities of absorbance of these proteins at known concentrations can be used to calculate the average field strength in tesla affecting the light path. Using these benchmarks along with corroboration from other members of the lab, an effective field strength of 2.5 T was decided to be used.

Protein samples of cytochrome *c* and myoglobin (equine heart) were prepared in a 100 mM Tris, 150 mM NaCl, pH 7.0 at concentrations of ~50 µM. For cytochrome *c*, the spectrum was recorded after the protein was fully reduced using excess NaDT, while myoglobin remained oxidised via air equilibration during the spectroscopic measurement. Samples of $MtrC_{Sol}^{Y657C\ H561M}$, $MtrC_{Sol}^{Y657C\ H561C}$, and $MtrC_{Sol}^{Y657C\ H230M}$ were prepared in a 100 mM Tris, 150 mM NaCl, pH 8.1 at ~10 µM. All protein samples were prepared aerobically before being transferred to an anaerobic chamber and placed in sealed cuvettes. Samples were placed into a 1 mm path length quartz cuvette and the spectrum was recorded with a longitudinal magnetic field in the forward and then reverse direction. The MCD spectra of all variants were measured while oxidised via air equilibration. This was followed by full reduction using excess NaDT before another set of spectra were taken. The following equation was used to provide Δε (M^{-1} cm^{-1} T^{-1}) values for each protein.

$$\frac{\frac{1}{2} \times (A_F - A_R)}{32980 \times c(M) \times 0.1\ (cm) \times 2.5\ (T)} = \Delta\varepsilon\ (M^{-1}\ cm^{-1}\ T^{-1})$$

Where A_F and A_R are the absorbance of left circularly polarised light minus the absorbance of right circularly polarised light at the specified wavelength (A_{LCP}–A_{RCP}) in forward and reverse fields

respectively, c is the protein molarity, and $\Delta\varepsilon$ is the molar absorption coefficient at the specified wavelength.

2.8 Protein crystallography

Crystals were obtained with the assistance of B. Nash under similar conditions to those of $MtrC_{Sol}$ via ninety-six well sitting drop vapour diffusion plates at 4°C (25). The reservoir solution used was 200 mM sodium acetate, 100 mM $CaCl_2$, 20% PEG 6000, pH 5.0, and the protein solution ~170 µM protein in 20 mM HEPES pH 7.8. The drop was injected with crystal seeds of $MtrC_{Sol}$. These were made by breaking up previously grown $MtrC_{Sol}$ protein crystals in the drop and diluting this further by 50× using the remaining reservoir solution. A total drop volume of 0.6 µL was formed by 0.05 µL crystal seeding solution, 0.3 µL protein solution, and 0.25 µL reservoir solution. Crystals were harvested and cryogenically protected by transfer into a reservoir solution containing 20% ethylene glycol before being plunged into liquid nitrogen. X-ray diffraction data was collected at the UK Diamond Light Source synchrotron on beamline I04. The X-ray scattering data was processed using Xia2 software and the resulting data sets were phased by molecular replacement in Phaser (49, 50). The structure of $MtrC_{Sol}$ (PDB: 4LM8) was used as the template for the generation of phases (25).

2.9 Protein film electrochemistry

Protein film electrochemical measurements were performed with the assistance of A. Sutton-Cook in a home-built electrochemical cell using a three electrode setup: a silver-silver chloride saturated with KCl reference electrode, a platinum counter electrode, and a protein-adsorbed mesoporous indium tin oxide (ITO) working electrode (prepared according to Mersch *et al.* (51)). The cell was set up in an anaerobic chamber and was surrounded by a Faraday cage to reduce interference from external electrical noise. A sample of each protein was made to ~40 µM in 100 mM Tris, 150 mM NaCl, pH 8.0, of which 5 µL was dispensed onto the indium doped tin oxide patch of the ITO working electrode. This was left in a petri dish on ice for fifteen minutes before being transferred into the anaerobic chamber containing the electrochemical cell. The non-adsorbed protein was washed from the electrode using 3×2 mL of an anaerobic solution of 100 mM NaCl, 50 mM HEPES, pH 8.0. The protein adsorbed electrode was subsequently submerged in the buffer-electrolyte solution and connected to the circuit. A scan rate of 20 mV/s was used with a start potential of -29 mV, upper potential of -9 mV and a lower potential of -809 mV. Cyclic voltammograms were produced by an Autolab PGSTAT30 using the NOVA 2.1.4 software. The voltammograms were baseline corrected using the Q-SOAS software (52). Potentials converted from vs KCl saturated silver-silver chloride electrode to vs SHE by the addition of +0.197 V.

Chapter 3. Preparation of novel hemoproteins

The results presented in this chapter detail the preparation of the plasmids pBAD.$C_{Sol}^{Y657C\ H561C}$, pBAD.$C_{Sol}^{Y657C\ H230M}$, and pBAD.$C_{Sol}^{Y657C\ H230C}$, and the attempted purification of their corresponding gene products $MtrC_{Sol}^{Y657C\ H561C}$, $MtrC_{Sol}^{Y657C\ H230M}$, and $MtrC_{Sol}^{Y657C\ H230C}$. The production of the plasmids pBAD.C_{Sol}^{Y657C} and pBAD.$C_{Sol}^{Y657C\ H561M}$ and their corresponding gene products and has already been reported by van Wonderan *et al.* (7). These plasmids were recovered from storage and confirmed via sequencing, and the pBAD.C_{Sol}^{Y657C} plasmid was used as a template for following polymerase chain reactions (PCRs). The levels of expression of the secreted gene products from these novel plasmids were measured during L-arabinose induction in protein expression trials. Analysis via SDS-PAGE and the UV-Vis electronic absorption spectra of spent media samples from the expression trials were used to quantitatively assess levels of protein expression. Following on from this the gene products were purified using StrepTactin aided affinity chromatography and analysed again via SDS-PAGE to ensure the samples had not degraded during purification. Lastly, LC-MS and detailed UV-Vis electronic absorbance spectra were used to show that the new variants of $MtrC_{Sol}^{Y657C}$ produced in this work are of the expected mass and share the similar spectral features of low spin full length $MtrC_{Sol}^{Y657C}$.

3.1 Preparation of plasmids encoding for $MtrC_{Sol}$ variants

The plasmids pBAD.C_{Sol}^{Y657C} and pBAD.$C_{Sol}^{Y657C\ H561M}$ have previously been produced and well characterised (7). These plasmids were recovered from -20°C storage and had their sequences confirmed via plasmid sequencing. The plasmid pBAD.C_{Sol}^{Y657C} was used as the template DNA for all following PCRs. All sequencing and mutagenic primers used to produce the plasmids used in this work are shown in **Table 1.**

PCR was chosen as the method to introduce the relevant point mutations into the pBAD.C_{Sol}^{Y657C} plasmid. Complimentary mutagenic primers were designed to have similar melting temperatures to each other, and to facilitate the two-step PCR protocol detailed by the Thermo Scientific Phusion Flash High-Fidelity PCR Master Mix manual (Thermo-fisher). A temperature gradient was used around the predicted melting temperature (Eurofins) of the primers. The PCR products were loaded onto a 0.8% DNA agarose gel and all samples across the temperature gradient migrated through the gel in the expected range of circularised plasmidic pBAD.C_{Sol}^{Y657C} of mass 6507 base pairs, suggesting the plasmids are full length. Once sent for sequencing it became apparent that issues with the primer design or the protocol was causing repeated inserts of sequences comparable to the mutagenic primers to be incorporated downstream of the intended mutation site. The experiment was repeated under different conditions, but only the plasmid pBAD.$C_{Sol}^{Y657C\ H561C}$ was successfully produced using primers Kr01 For and Kr02 Rev (**Figure 11A**). The remaining mutagenic primers were re-designed using methods developed by Naismith *et al.* (53), and the PCRs to produce pBAD.$C_{Sol}^{Y657C\ H230M}$ and pBAD.$C_{Sol}^{Y657C\ H230C}$ were re-attempted. The resulting DNA agarose gel suggested full length plasmid had been produced (**Figure 11B** and **11C**), and when the sequence data was returned it showed incorporation of the desired point mutation using Kr03 For and Kr04 Rev (pBAD.$C_{Sol}^{Y657C\ H230M}$), and Kr05 For and Kr06 Rev (pBAD.$C_{Sol}^{Y657C\ H230C}$) with no undesired mutations. The plasmids were electroporated into *S. oneidensis* using methods previously described (28) and protein expression trials were conducted.

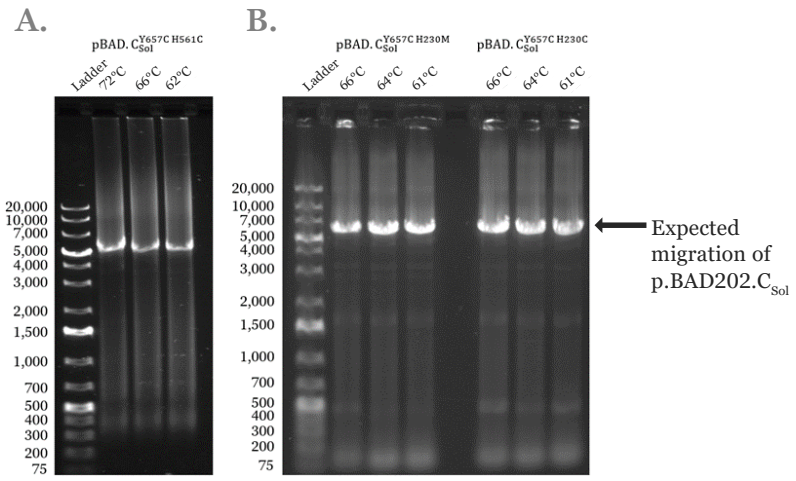

Figure 11. DNA agarose gels from the PCR of production of **A)** pBAD.$C_{Sol}^{Y657C\ H561C}$, **B)** pBAD.$C_{Sol}^{Y657C\ H230M}$, and **C)** pBAD.$C_{Sol}^{Y657C\ H230C}$. The temperature of each reaction is used to label the lanes.

3.2 Protein expression

In order to assess the levels and favoured conditions of expression for the novel $MtrC_{Sol}^{Y657C}$ variants $MtrC_{Sol}^{Y657C\ H561C}$, $MtrC_{Sol}^{Y657C\ H230M}$, and $MtrC_{Sol}^{Y657C\ H230C}$ an experiment was conducted where the concentration of the inducer L-arabinose was varied across otherwise identical growth conditions. For this experiment the soluble nature of $MtrC_{Sol}$ and the fact it is excreted into the media during cell growth was exploited. Once the cells had been induced with L-arabinose and had grown overnight the culture was centrifuged to remove the cells, and the supernatant was collected. The UV-Vis electronic absorbance of the spent media was recorded and showed all samples, excluding the 0 mM L-arabinose

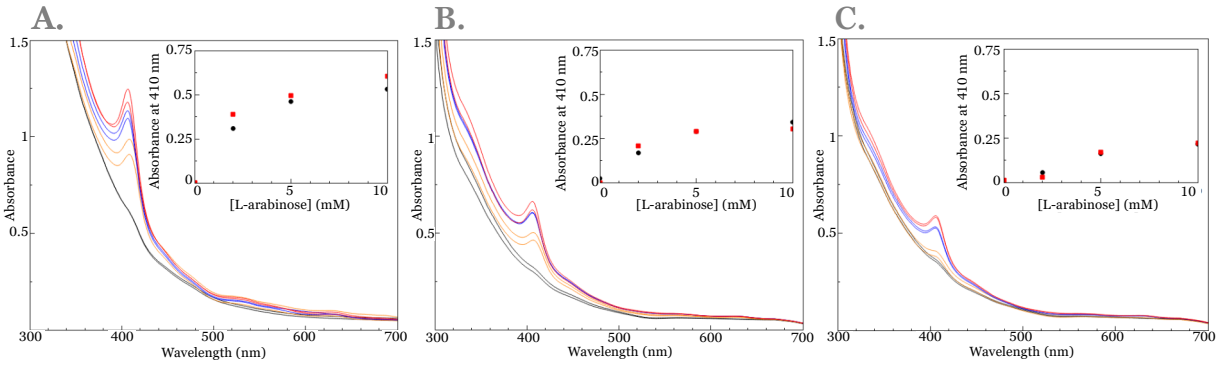

Figure 12. Protein expression trial spectra of spent media samples **A)** $MtrC_{Sol}^{Y657C\ H561C}$, **B)** $MtrC_{Sol}^{Y657C\ H230M}$, and **C)** $MtrC_{Sol}^{Y657C\ H230C}$. The colours represent concentrations of L-arabinose during growth and are as follows: black = 0 mM, yellow = 2 mM, blue = 5 mM, red = 10 mM. Insert is the absorbance of each sample at 410 nm (Soret peak) with the 410 nm absorbance of a 0 mM L-arabinose induced sample removed.

induced ones, have a substantial Soret peak at 410 nm characteristic of oxidised $MtrC_{Sol}$ (**Figure 12**). The highest intensity electronic absorbance at 410 nm of each sample is seen in the 10 mM L-arabinose induced cultures. This suggests that higher concentrations of L-arabinose are correlated with higher concentrations of excreted heme. However, as previously discussed *S. oneidensis* MR-1

has a wide array of heme containing proteins used in its extracellular electron transport pathway. It is quite possible that the heme absorbance seen in the samples with a high L-arabinose concentration is not originating from the desired full length gene product of the transformed plasmid, but rather from a degraded form of the protein or other cytochromes released during cell lysis (such as FccA or STC). To determine whether this was the case samples were analysed via SDS-PAGE. Both the Coomassie and heme stained SDS-PAGE gels indicate the presence of a protein band migrating as expected for $MtrC_{Sol}$ on non-reducing SDS-PAGE gels (**Figure 13**). Although $MtrC_{Sol}$ is a 76 kDa protein, it is always seen at a lower mass of around 70-74 kDa on non-reducing SDS-PAGE gels, justified by considering the nature of the covalently bound hemes and disulphide bridge in domain III not allowing the protein to fully unfold. $MtrC_{Sol}$ run on SDS-PAGE can be seen in **Figure 15D** for reference. The intensity of the band at this mass is highest at 2 mM L-arabinose. The 5 and 10 mM L-arabinose samples have heavy heme staining at very low masses (<10 kDa) suggesting the presence of a degraded form of a hemoprotein. This supports the idea that higher concentrations of L-arabinose are stressing the cells during growth and causing the release of undesired or truncated products. For this reason, 2 mM of

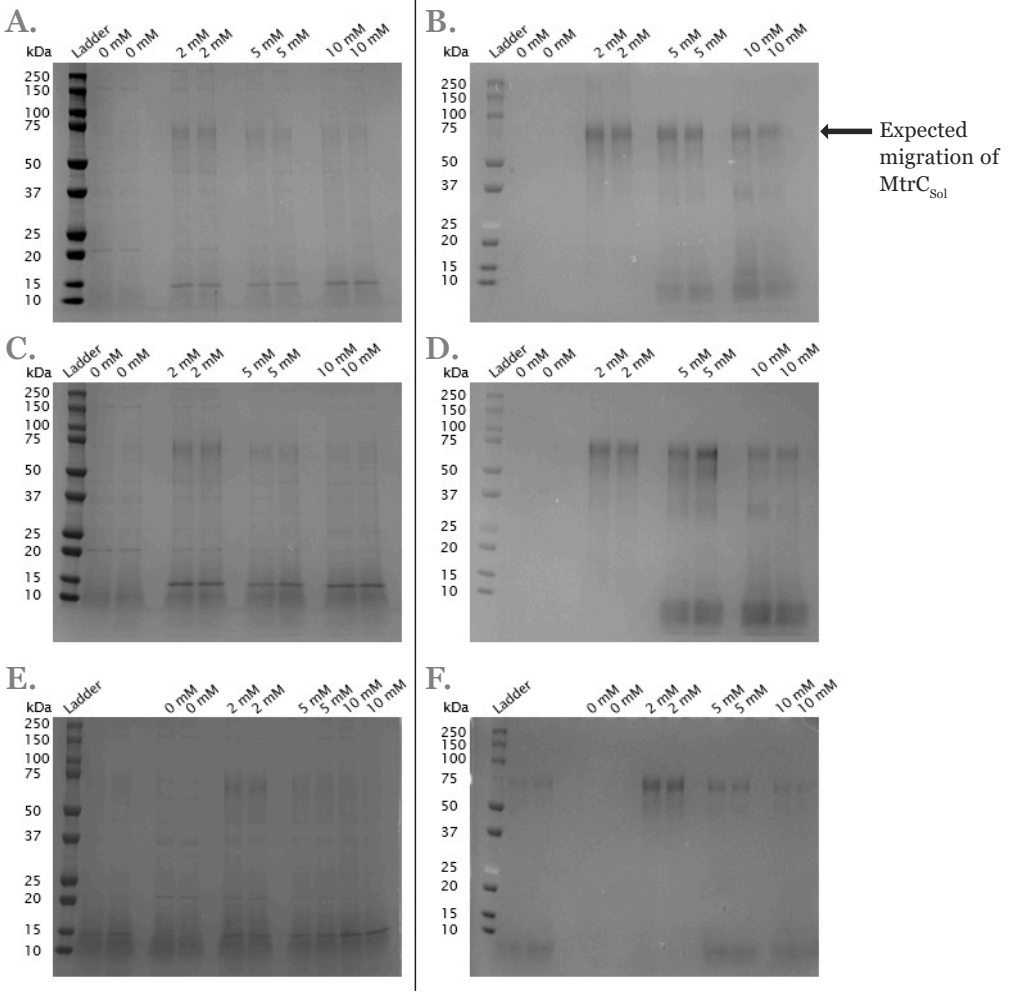

Figure 13. Protein expression trial SDS-PAGE gel images stained with Coomassie brilliant blue (left) and a heme stain (right). **A&B)** $MtrC_{Sol}^{Y657C\ H561C}$, **C&D)** $MtrC_{Sol}^{Y657C\ H230M}$, and **E&F)** $MtrC_{Sol}^{Y657C\ H230C}$. Gel lanes are the product of varying levels of L-arabinose induction. Concentration of L-arabinose is seen increasing in concentration across the top of the gel and is indicated for each lane. Experiments were performed in duplicate for each L-arabinose concentration. The unlabelled lanes of E&F are from a different experiment.

L-arabinose was chosen as the concentration for induction during experiments that aimed to produce and then purify the desired proteins in this work.

3.3 Protein purification

StrepII tag aided affinity chromatography was used in the attempted purification of the variants $MtrC_{Sol}^{Y657C\ H561C}$, $MtrC_{Sol}^{Y657C\ H230M}$, and $MtrC_{Sol}^{Y657C\ H230C}$. The spent media from the cultures were loaded onto a StrepTactin column to bind any material containing a StrepII tag. The StrepTactin column turned bright red during the loading of the spent media for all samples (**Figure 14**), suggesting the binding of heme containing material which is consistent with the expressed gene product. The eluted samples were analysed via SDS-PAGE alongside a sample of the spent media (pre-column) and the material that passed over but did not bind to the column (flow-through) (**Figure 15**). A sample of

Figure 14. Three StrepTactin columns in series becoming saturated with red material during the loading of spent media, consistent with the expected gene products.

$MtrC_{Sol}^{Y657C}$ that had been previously purified and confirmed to be full length via mass spectrometry was used as a migration indicator to where the purified sample should be seen on non-reducing SDS-PAGE gels. Both the Coomassie and heme stained gel images of the purified samples from plasmids $pBAD.C_{Sol}^{Y657C\ H561C}$ and $pBAD.C_{Sol}^{Y657C\ H230M}$ show banding at the same migration as $MtrC_{Sol}^{Y657C}$. Banding at a comparable migration can also be seen in the pre-column and flow-through sample lanes. The banding in the flow-though lane is very weak compared to that of the pre-column samples, suggesting that the majority of the material at this mass has bound to the StrepTactin column and been released during the elution step. From this point forwards, the samples purified here will be referred to as $MtrC_{Sol}^{Y657C\ H561C}$ and $MtrC_{Sol}^{Y657C\ H230M}$.

During the protein expression trials in section 3.2 a full length gene product of $pBAD.C_{Sol}^{Y657C\ H230C}$ appears to be present on both the Coomassie and heme stained SDS-PAGE gels (**Figure 12**). However, after StrepTactin purification no such band appears in any gel lane containing the eluted protein (**Figure 15C**). In the purified sample lane there is a prominent band at ~50 kDa. Since this material should have a StrepII tag as it has bound to and been eluted from the StrepTactin column, it is likely

that a degraded form of the protein has been purified. Although these experiments were intended to be performed in an identical manner to each other, the purification of the pBAD.$C_{Sol}^{Y657C\ H230C}$ gene product was re-attempted to eliminate experimental differences. Unfortunately, the same result was observed and consequently production of the protein was not explored further.

The purified sample lanes of $MtrC_{Sol}^{Y657C\ H561C}$ and $MtrC_{Sol}^{Y657C\ H230M}$ (**Figure 15A&B**) have additional bands at lower masses than the expected mass of the full length product, seen primarily in the heme stained gel. Although the intensity of these bands is likely exaggerated due to the nature of the heme stain (the heme stain is catalytic and prone to over-staining the gel, evidenced by the presence of the same band in the already purified $MtrC_{Sol}^{Y657C}$ sample), the potential for these contaminants to interfere with future experiments was not ignored. Consequently, the purified $MtrC_{Sol}^{Y657C\ H561C}$ and $MtrC_{Sol}^{Y657C\ H230M}$ samples were run through a size exclusion column to remove these potentially truncated versions of the full length protein. It should also be noted that there is the faint presence of a band at ~150 kDa seen in the $MtrC_{Sol}^{Y657C}$ lanes of the heme stained gels. This band is ubiquitous among samples containing the Y657C substitution run on non-reducing SDS-PAGE (7). Due to the nature of this substitution presenting a free cysteine on the protein surface the cell is thought to cap this cysteine with a protecting group to prevent unwanted reactions during secretion (see section 1.5). It is concluded that the presence of this 150 kDa band is representative of a small percentage of the

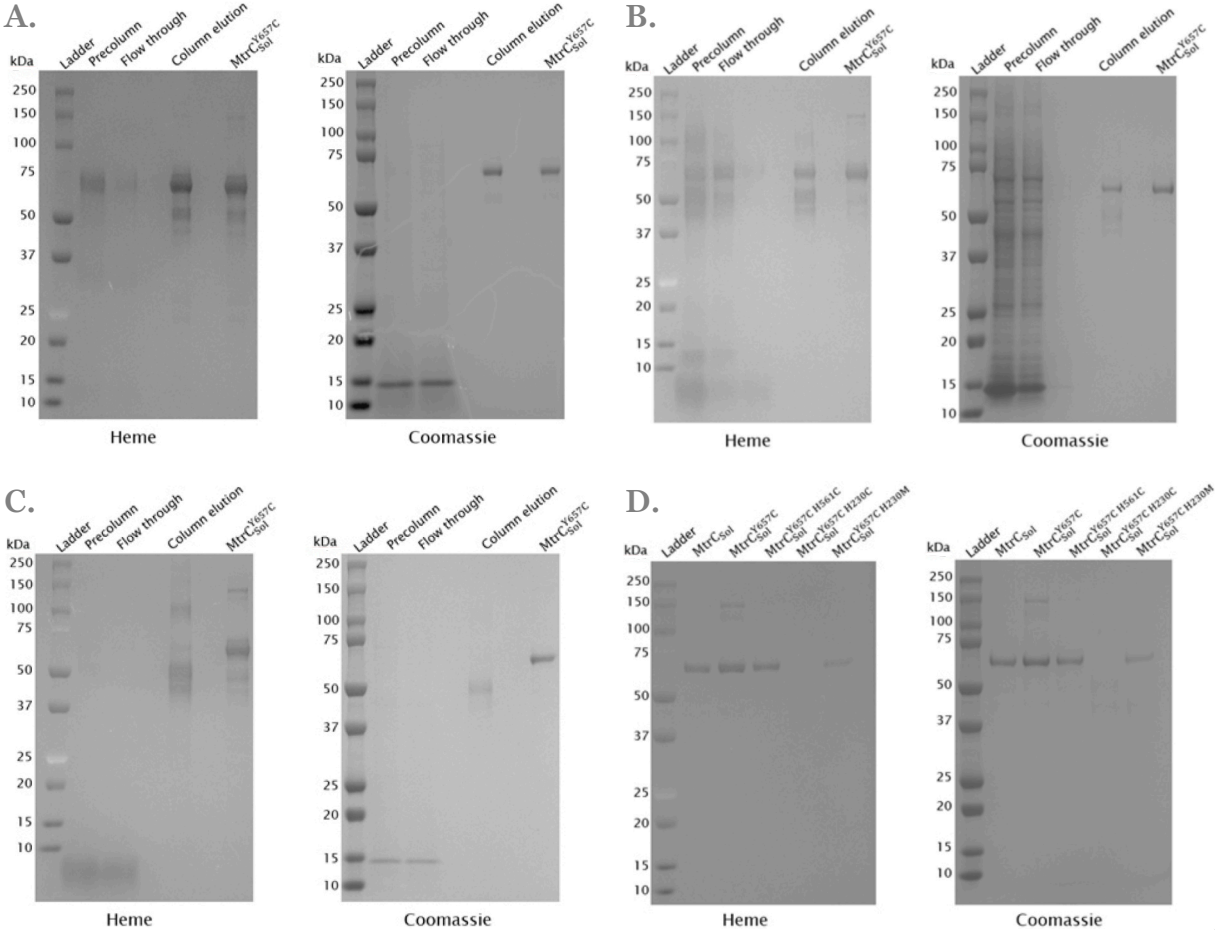

Figure 15. SDS-PAGE gel images of samples obtained at various stages of the purification of **A)** $MtrC_{Sol}^{Y657C\ H561C}$, **B)** $MtrC_{Sol}^{Y657C\ H230M}$, and **C)** $MtrC_{Sol}^{Y657C\ H230C}$. **D)** Samples of purified material from each protein purification are run side by side, as well as $MtrC_{Sol}^{Y657C}$ and $MtrC_{Sol}$ for migration comparison. Gels stained with both heme (left) and Coomassie (right) are available.

proteins that did not receive this cysteine cap and have formed disulfide bridge mediated dimers. Again, this band is likely emphasised by the sensitive nature of the heme stain, and the presence of these dimers should not impact future experiments. These dimers are removed during gel filtration but may be reformed if the cysteine cap is removed.

A final set of Coomassie and heme stained gel images are presented in **Figure 15D** which contain samples of $MtrC_{Sol}$, $MtrC_{Sol}^{Y657C}$, and the novel proteins discussed in this section. Fresh samples of $MtrC_{Sol}^{Y657C}$ and $MtrC_{Sol}^{Y657C\ H561M}$ were purified using the same techniques as the novel proteins discussed in this section and are used in experiments from this point forwards. The results of these purifications are as expected and in agreement with those previously published and are therefore not presented here (7).

The yields for $MtrC_{Sol}^{Y657C\ H561C}$ and $MtrC_{Sol}^{Y657C\ H230M}$ were 6.3 mg/L and 2.5 mg/L respectively (spectra presented in the next section). The yield for $MtrC_{Sol}^{Y657C\ H561C}$ lies within the expected amount typical of $MtrC_{Sol}$ (5-10 mg/L) (28). $MtrC_{Sol}^{Y657C\ H230M}$ has almost half the minimum expected yield for $MtrC_{Sol}$, however enough protein was produced to continue with further experiments. It is unclear why the yield is so much lower for $MtrC_{Sol}^{Y657C\ H230M}$ than $MtrC_{Sol}^{Y657C\ H561C}$. Repeated experiments would be needed to determine how reproducible these values are.

3.4 Analysis of purified gene products

The StrepTactin column turning red during purification and the eluted material having strong 410 nm electronic absorbance is in concordance with successfully expressed gene product for the plasmids produced (detailed in section 2.1). The SDS-PAGE gel images show the purified products of plasmids $pBAD.C_{Sol}^{Y657C\ H561C}$ and $pBAD.C_{Sol}^{Y657C\ H230M}$ has heme containing material that migrates through the gel to the same position as $MtrC_{Sol}^{Y657C}$. This product can be purified further via size exclusion chromatography to produce a single band at the expected migration for pure $MtrC_{Sol}^{Y657C}$. At this point the protein is considered successfully expressed and purified, however an accurate mass is required to ensure no changes have been made that is undetectable on SDS-PAGE. To achieve this, LC-MS is utilised to provide an accurate value for the intact mass of each protein. Since most of these proteins

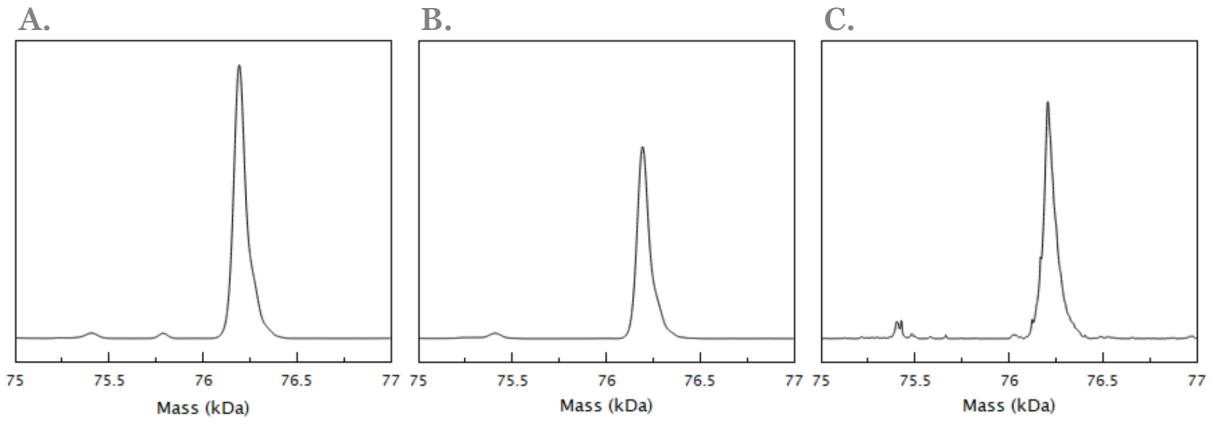

Figure 16. Deconvoluted LC-MS trace of intact masses for **A)** $MtrC_{Sol}^{Y657C\ H561M}$ (predicted: 76,185 Da, observed: 76,186 Da), **B)** $MtrC_{Sol}^{Y657C\ H230M}$ (predicted: 76,185 Da, observed: 76,186 Da), and **C)** $MtrC_{Sol}^{Y657C\ H561C}$ (predicted: 76,158 Da, observed: 76,209 Da).

express with an unknown protecting group on the surface cysteine introduced at the Y657 position, the samples were treated with TCEP before analysis (7). This will reduce any surface covalent cysteine modification and allow for the observed mass to be accurately correlated to the calculated mass of the fully maturated cytochrome. The predicted mass of each protein as well as the measured mass is available in **Figure 16**.

The mass of $MtrC_{Sol}^{Y657C\ H561M}$ and $MtrC_{Sol}^{Y657C\ H230M}$ are identical as expected when considering the substitutions made to each are the same, just at two different positions. The masses of these two proteins are within reasonable error of the predicted mass which confirms the successful incorporation of ten *c*-type hemes and the desired amino acid substitution. However $MtrC_{Sol}^{Y657C\ H561C}$ is +51 Da larger than expected. This mass difference is best explained when considering the consequences of introduction of a free cysteine into the amino acid chain. If the cysteine introduced at position 561 is covalently modified, TCEP treatment may not affect it due to it being buried in the tertiary protein structure, resulting in a higher observed mass. Due to this mass difference not being easily explainable by amino acid substitutions or protein degradation, the $MtrC_{Sol}^{Y657C\ H561C}$ protein is treated as full length. Further evidence for covalent modification to the cysteine at position 561 is discussed in section 4.2.

A set of UV-Vis electronic absorption spectra were attained to offer insight into the general protein fold and ligation of the hemes in $MtrC_{Sol}^{Y657C}$, $MtrC_{Sol}^{Y657C\ H561M}$, $MtrC_{Sol}^{Y657C\ H561C}$, and $MtrC_{Sol}^{Y657C\ H230M}$ (**Figure 17**). The spectra of the oxidised and reduced protein variants are similar to that of $MtrC_{Sol}$ (28). Although not diagnostic, this suggests no substantial changes to the tertiary protein structure or

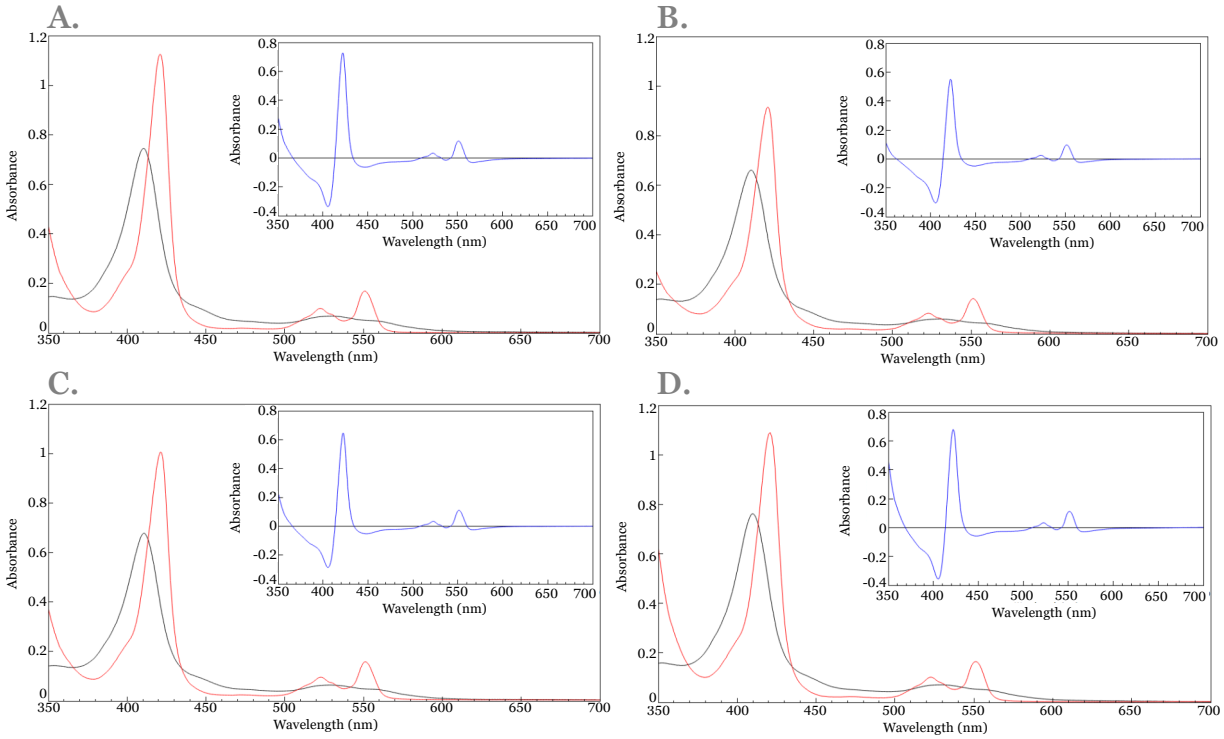

Figure 17. The UV-Vis electronic absorbance spectra of **A)** $MtrC_{Sol}^{Y657C}$, **B)** $MtrC_{Sol}^{Y657C\ H561C}$, **C)** $MtrC_{Sol}^{Y657C\ H561M}$, and **D)** $MtrC_{Sol}^{Y657C\ H230M}$. The black trace is protein oxidised via air equilibration, and the red trace is after full reduction using excess NaDT. Insert (blue trace) is an oxidised-reduced difference spectrum. All samples recorded in 100 mM Tris, 150 mM NaCl, pH 8.1.

heme environment. As discussed in chapter 1, the absorption spectrum of hemoproteins is dominated by π-π* porphyrin transitions (Soret band). However, smaller spectral features are produced by charge transitions from the axial ligand to the iron centre. These features are usually masked by the intense Soret absorbance peak but are often seen in a difference spectrum. High spin heme in $MtrC_{Sol}$ has inadvertently been produced previously (van Wonderen, unpublished), and a spectral feature at 440 nm is observed in the reduced–oxidised difference spectrum of these proteins (54). The absence of such features is a positive indicator that all hemes in the proteins produced in this work are low spin. However, much more sensitive spectroscopy is required to be truly diagnostic of the heme spin state in these proteins, such as MCD, discussed in chapter 4.

In order to determine accurate extinction coefficients for the new MtrC variants, a pyridine hemochromagen experiment was performed. The measured extinction coefficients at specified wavelengths are generally comparable between protein variants (**Table 4**). The extinction coefficients for $MtrC_{Sol}^{Y657C\ H561C}$ and $MtrC_{Sol}^{Y657C\ H561M}$ are similar, with $MtrC_{Sol}^{Y657C\ H561C}$ having a trend of being slightly lower than that of $MtrC_{Sol}^{Y657C\ H561M}$. $MtrC_{Sol}^{Y657C\ H230M}$ seems to have coefficients that are the most different to the other variants, possibly explained by the unique feature of an altered heme three environment. The presented extinction coefficients in **Table 4** are at the same wavelengths as those presented in the supplementary information of van Wonderen *et al.* (7). This is to aid in measuring the level of agreement between the two sets of data. Although the measured extinction coefficients in van Wonderen *et al.* (7) do not entirely agree with the results presented here, the difference is small and consequently the extinction coefficients produced in this work are the ones used moving forwards. The results obtained here are consistent with the hypothesis that the extinction coefficients would change for the $MtrC_{Sol}^{Y657C}$ variants with altered heme environments

Table 4. *Measured extinction coefficients for the fully folded $MtrC_{Sol}^{Y657C}$ variants as determined by the pyridine hemochromagen assay. Three technical repeats were performed for each protein. Standard error is shown as a ± value.*

	Extinction coefficient ($mM^{-1}\ cm^{-1}$)			
Protein name	**Ox at 410 nm**	**Red at 420 nm**	**421–405 nm**	**552–568 nm**
$MtrC_{Sol}^{Y657C}$	1330 ± 12	1990 ± 17	1854 ± 16	260 ±2
$MtrC_{Sol}^{Y657C\ H561M}$	1280 ± 9	1869 ±14	1698 ± 12	251 ± 2
$MtrC_{Sol}^{Y657C\ H561C}$	1280 ± 25	1757 ± 34	1616 ± 31	232 ± 4
$MtrC_{Sol}^{Y657C\ H230M}$	1371 ± 3	1951 ± 5	1831 ± 4	253 ± 1

3.5 Summary

This chapter presents work that aimed to produce the$MtrC_{Sol}^{Y657C\ H561C}$, $MtrC_{Sol}^{Y657C\ H230M}$ and $MtrC_{Sol}^{Y657C\ H230C}$ proteins. A combination of protein expression trials, purification, and spectroscopic and biochemical analysis has confirmed the production $MtrC_{Sol}^{Y657C\ H561C}$ and $MtrC_{Sol}^{Y657C\ H230M}$. The intact protein mass for $MtrC_{Sol}^{Y657C\ H230M}$ matches the calculated mass, while there appears to be a +51 Da larger than expected observed intact mass for $MtrC_{Sol}^{Y657C\ H561C}$. This is rationalised as post translational covalent cysteine modification to the cysteine at position 561, although no evidence is yet presented to support this. The measured extinction coefficients are in line with what was expected and not substantially different from those published. UV-Vis electronic absorbance spectroscopy of both $MtrC_{Sol}^{Y657C\ H561C}$ and $MtrC_{Sol}^{Y657C\ H230M}$ is consistent with all ten hemes being low spin, and therefore having octahedral ligation.

A plasmid encoding for $MtrC_{Sol}^{Y657C\ H230C}$ was successfully prepared. However, it was not possible to find evidence for the purification of the desired gene product. Instead, a heme containing protein with the C-terminal StrepII tag was purified, possibly a truncated form of the $MtrC_{Sol}^{Y657C\ H230C}$ protein. Although the full length protein was evident during expression trials, it does not appear to tolerate the harsher conditions during purification.

Chapter 4. Characterisation of novel proteins

In the previous chapter the successful purification of the proteins $MtrC_{Sol}^{Y657C}$, $MtrC_{Sol}^{Y657C\ H561M}$, $MtrC_{Sol}^{Y657C\ H561C}$, and $MtrC_{Sol}^{Y657C\ H230M}$ is discussed. At this point it is considered that the introduction of the desired substitutions has been successful into these proteins, and that the proteins are full length. However, the ligands to the hemes in the variant $MtrC_{Sol}^{Y657C}$ proteins are undefined. The UV-Vis electronic absorbance spectra of the variant $MtrC_{Sol}^{Y657C}$ proteins did not offer any evidence of high spin heme, consistent with the ten His/His ligated hemes of $MtrC_{Sol}^{Y657C}$. However, in a ten heme protein the presence of the high spin spectral indicators may be buried in absorbance peaks of the other nine low-spin hemes. In this chapter magnetic circular dichroism is used as a more sensitive diagnostic tool to probe the spin state of the ten hemes in each protein in solution in a way that cannot be masked by the presence of low spin heme. Also presented are structures defined by X-ray crystallography. These structures are used to analyse electron density around the iron of hemes three and eight, and to support the conclusions drawn from MCD concerning the potential covalent cysteine modifications to the Y657C and H561C substitutions. The chapter is concluded with results from protein film voltammetry that provide an indication of the redox properties of these proteins.

4.1 Magnetic circular dichroism

Circular dichroism (CD) is a highly sensitive analytical technique that probes electron transitions when energy from left and right circularly polarised light is differentially absorbed in intrinsically chiral molecules. By introducing a parallel magnetic field to the direction of light propagation during CD, and taking a forward field minus reverse field difference, a spectrum is produced that accurately reports the spin state of the hemes. This spectrum has the natural CD observed in the highly chiral protein removed resulting in a reliable and easily interpretable analytical technique. High spin heme presents itself clearly on an MCD spectra of oxidised room temperature sample as a small negative peak at 640 nm, as seen in the MCD spectra of air equilibrated horse heart myoglobin (**Figure 18A**). This feature is not seen on MCD spectra of low spin heme, such as that of cytochrome c (**Figure 18B**). Analysis of the MCD spectra shows that the proteins $MtrC_{Sol}^{Y657C}$, $MtrC_{Sol}^{Y657C\ H561M}$, $MtrC_{Sol}^{Y657C\ H561C}$, and $MtrC_{Sol}^{Y657C\ H230M}$ contain no evidence of high-spin heme (**Figure 18**). The features seen in the reduced form of each protein are comparable to the low spin reduced form of horse heart cytochrome *c*. This suggests all hemes are in full octahedral coordination with two strong field axial ligands. A water molecule constitutes a weak field ligand and would likely take the place of an amino acid side chain as the distal ligand if coordination by an amino acid had not occurred. A water molecule can therefore be ruled out as a potential ligand.

4.2 X-ray crystallography

Previous attempts to produce protein crystals of $MtrC_{Sol}^{Y657C}$ and $MtrC_{Sol}^{Y657C\ H561M}$ have been unsuccessful. This was attributed to the surface cysteine residue in the 657 positions in both versions of the protein interfering with the crystallisation. Crystals of $MtrC_{Sol}^{H561M}$ without the Y657C substitution were made to support the evidence of successful methionine ligation to the heme (7). In this work, successful crystal growth of proteins containing the Y657C substitution was achieved by crystal seeding. Previously grown $MtrC_{Sol}$ crystals were harvested, shattered, and added to the crystallisation drop. This addition of a nucleation point allowed for crystal growth across all variants of $MtrC_{Sol}^{Y657C}$. Diffraction data was collected for the full roster of $MtrC_{Sol}^{Y657C}$, $MtrC_{Sol}^{Y657C\ H561M}$, $MtrC_{Sol}^{Y657C\ H561C}$, and $MtrC_{Sol}^{Y657C\ H230M}$ proteins. Data collection and refinement statistics are available in **Table 5**.

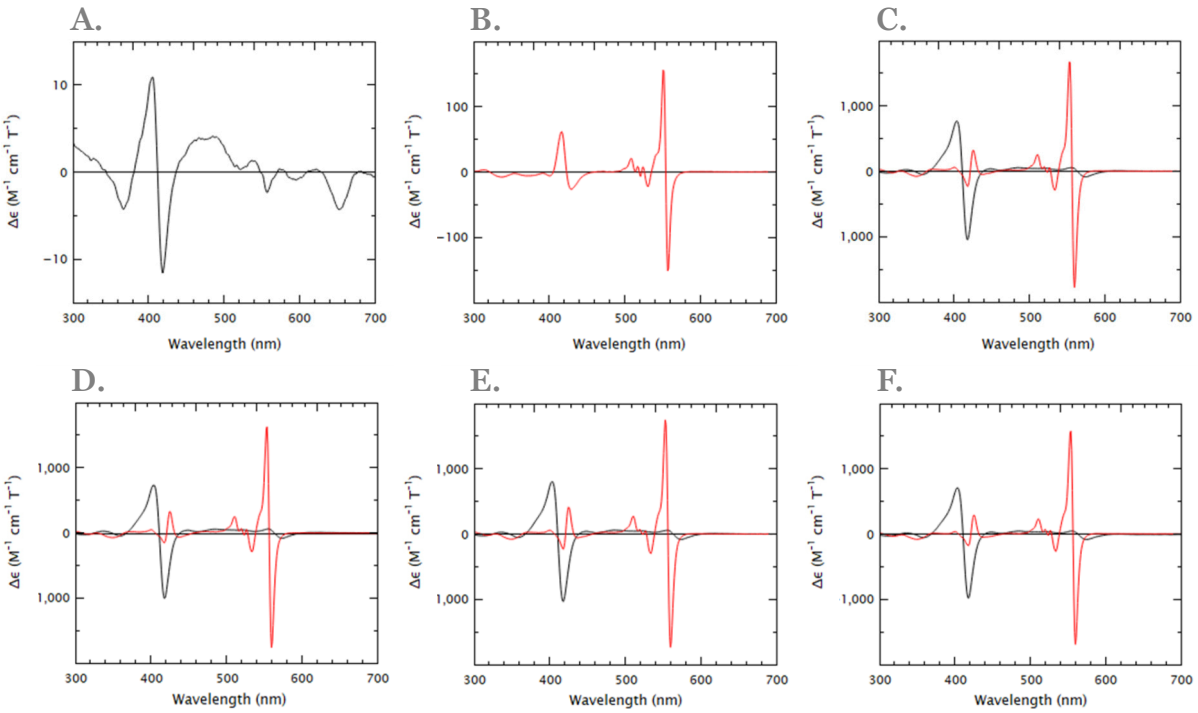

Figure 18. MCD of proteins **A)** HH Myoglobin, **B)** HH Cytochrome c, **C)** $MtrC_{Sol}^{Y657C}$, **D)** $MtrC_{Sol}^{Y657C\ H561M}$, **E)** $MtrC_{Sol}^{Y657C\ H230M}$, and **F)** $MtrC_{Sol}^{Y657C\ H561C}$. The black trace is protein oxidised via air equilibration, and the red trace is after full reduction using excess NaDT.

Preliminary analysis of the X-ray diffraction data of all proteins shows the structures of $MtrC_{Sol}^{Y657C}$, $MtrC_{Sol}^{Y657C\ H561M}$, $MtrC_{Sol}^{Y657C\ H561C}$, and $MtrC_{Sol}^{Y657C\ H230M}$ overlay the structure of $MtrC_{Sol}$ (PDB: 4LM8) with no substantial changes to the protein fold or overall tertiary structure (**Figure 19A**). All four proteins contain the ten hemes of the heme wire, bound by the expected CXXCH motif seen in $MtrC_{Sol}$. Zooming in closer to the 657 residue shows the electron density of the resolved proteins do not match the structure of $MtrC_{Sol}$. The tyrosine residue at position 657 offers far too much electron density, and there is missing density seen nearby (**Figure 19B**). Mutating the $MtrC_{Sol}$ structure in silico to include a cysteine at position 657 and running refinement presents a much better fit (**Figure 19 C&D**). There is clearly still missing density here, which is expected in samples without the covalent cysteine modifications removed, such as the ones used to grow these crystals. This increased electron density is thought to be due to covalent modification through disulphide bonding to C657 (7). The conclusion drawn here is that successful insertion of a cysteine into the CXXCH binding motif of heme ten has not had a discernible impact on protein fold and heme ligation. This has resulted in a unique CXCCH binding motif in the $MtrC_{Sol}^{Y657C}$ protein and its variants.

Mapping the resolved electron density of the $MtrC_{Sol}^{Y657C\ H561M}$, $MtrC_{Sol}^{Y657C\ H561C}$, and $MtrC_{Sol}^{Y657C\ H230M}$ protein variants onto the structure of $MtrC_{Sol}$ revealed some key observations regarding heme binding ligands. For nine of the ten hemes in the structure, heme binding was unaffected and they remained His/His ligated. The only differences in heme ligation observed are where distal heme ligands have been substituted. In the $MtrC_{Sol}^{Y657C\ H230M}$ variant, the distal histidine ligand of heme three did not fit well with the observed electron density. Similarly, for the $MtrC_{Sol}^{Y657C\ H561M}$ and $MtrC_{Sol}^{Y657C\ H561C}$ variants, the distal histidine ligand of heme eight also appeared to be a poor fit for the electron density map. After mutating the $MtrC_{Sol}$ structure to include the relevant substitutions, the methionine residues in $MtrC_{Sol}^{Y657C\ H561M}$ (**Figure 20A**) and $MtrC_{Sol}^{Y657C\ H230M}$ (**Figure 20B**) appear to fit the

electron density well, and the $MtrC_{Sol}^{Y657C\ H230M}$ structure is comparable to that of $MtrC_{Sol}^{Y657C\ H561M}$. The distance between the sulphur of the distal methionine and the iron centre of the heme is 2.7 Å in $MtrC_{Sol}^{Y657C\ H230M}$, and 2.5 Å in $MtrC_{Sol}^{Y657C\ H561M}$, strongly suggesting successful ligation.

Table 5. *Protein crystal data collection and refinement statistics.*

	$MtrC_{Sol}^{Y657C}$	$MtrC_{Sol}^{Y657C\ H561M}$	$MtrC_{Sol}^{Y657C\ H561C}$	$MtrC_{Sol}^{Y657C\ H230M}$
Space group	P 2_1 2_1 2_1	P 2_1 2_1 2_1	P 2_1 2_1 2_1	P 2_1 2_1 2_1
Cell dimensions				
a, *b*, *c* (Å)	52.92, 90.05, 155.16	52.93, 89.94, 154.98	53.03, 89.34, 154.97	53.18, 89.89, 154.67
α, *β*, *γ* (°)	90.00, 90.00, 90.00	90.00, 90.00, 90.00	90.00, 90.00, 90.00	90.00, 90.00, 90.00
Resolution (Å)	77.88 -2.401 (2.48 -2.4)	77.49-1.75 (1.79-1.75)	77.48-1.889 (1.94-1.89)	77.71-2.4 (2.48-2.4)
R_{work}	0.1885 (0.3612)	0.1972 (0.3900)	0.2001 (0.3404)	0.1950 (0.3128)
R_{free}	0.2552 (0.3978)	0.2291 (0.3631)	0.2498 (0.3615)	0.2686 (0.3709)
R.M.S				
Bonds (Å)	0.009	0.007	0.008	0.009
Angles (°)	1.1	0.95	0.95	1.08
Ramachandran outliers	0.16	0.32	0.32	0.00
No. of reflections	404630 (35519)	1019565 (62427)	854402 (59445)	404874 (37575)
R_{Merge}	0.452 (4.219)	0.2299 (3.041)	0.3953 (3.792)	0.7138 (4.015)
R_{pim}	0.1267 (1.188)	0.06413 (0.9014)	0.1098 (1.035)	0.1998 (1.102)
Mean I/sigma(I)	4.07 (0.39)	6.51 (0.42)	4.18 (0.36)	3.51 (0.63)
CC1/2	0.977 (0.32)	0.997 (0.362)	0.99 (0.372)	0.961 (0.351)
Completeness	99.49 (95.62)	99.63 (97.32)	99.83 (98.44)	99.84 (99.10)
Redundancy	13.6 (13.4)	13.5 (11.9)	13.7 (14.1)	13.6 (14.2)
Rotamer outliers	2.32	0.97	1.35	2.32
Clash score	6.81	3.3	3.51	5.31
Average B-factor	50.48	31.2	33.59	37.23
Macromolecules	51.01	31.34	33.72	37.68
Ligands	48.55	26.49	30.55	34.05
Solvent	42.13	34.03	35.21	34.52

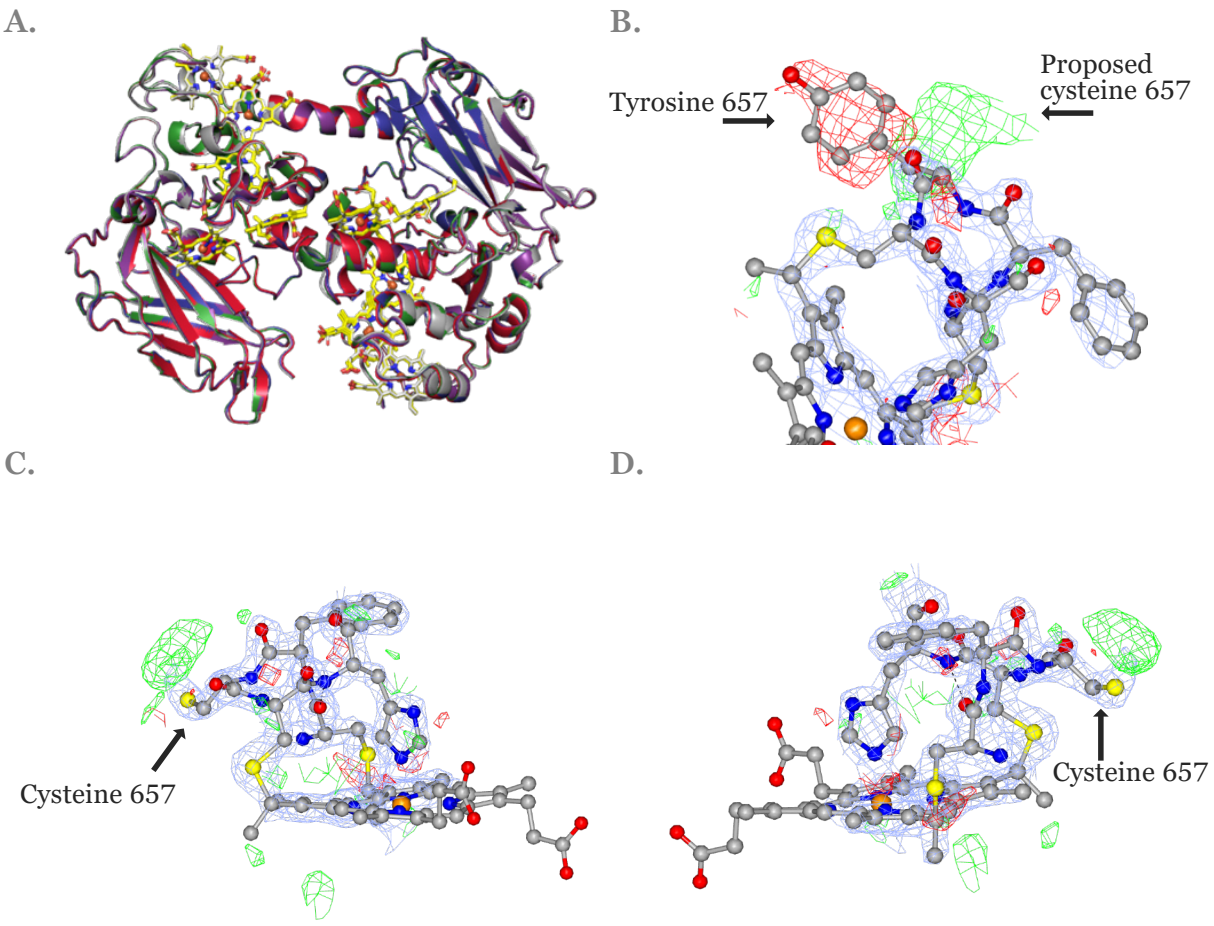

Figure 19. A) The resolved crystal structures, including the heme chains (yellow), of $MtrC_{Sol}^{Y657C}$ (green), $MtrC_{Sol}^{Y657C\ H561M}$ (red), $MtrC_{Sol}^{Y657C\ H561C}$ (blue), and $MtrC_{Sol}^{Y657C\ H230M}$ (purple) all overlayed with $MtrC_{Sol}$ (white, PDB: 4LM8) showing no major structural differences. **B)** The coordinates of $MtrC_{Sol}^{Y657C\ H561M}$ over the structure of $MtrC_{Sol}$ (PDB: 4LM8) at the 657 position near heme ten. **C&D)** Different angles of the same position as b) now with tyrosine mutated in sillico to a cysteine in the $MtrC_{Sol}$ structure. For b-d) a difference contour map (± 2.5 sigma) is shown where green is + 2.5 and red is - 2.5. Regular atom density maps are shown in light blue.

Comparing the $MtrC_{Sol}^{Y657C\ H561C}$ structure to its density map there is clearly missing electron density between the sulphur of the cysteine and the heme (**Figure 20C**). To ensure that this missing density is not filled with water or hydroxide, a water molecule was added to the structure in the middle of this density and the structure was re-refined. As shown in **Figure 20D** the water molecule does not offer enough density to make it a good fit. This is in agreement with the observations made during MCD analysis, which showed the absence of any features of high spin heme. The difference in predicted versus observed mass seen in $MtrC_{Sol}^{Y657C\ H561C}$ when analysed via LC-MS suggests there is mass that is observed but unaccounted for. This is also in concordance with this missing density, as this structural data seems to suggest that covalent modification of the cysteine at position 561 is the group that has ligated the heme.

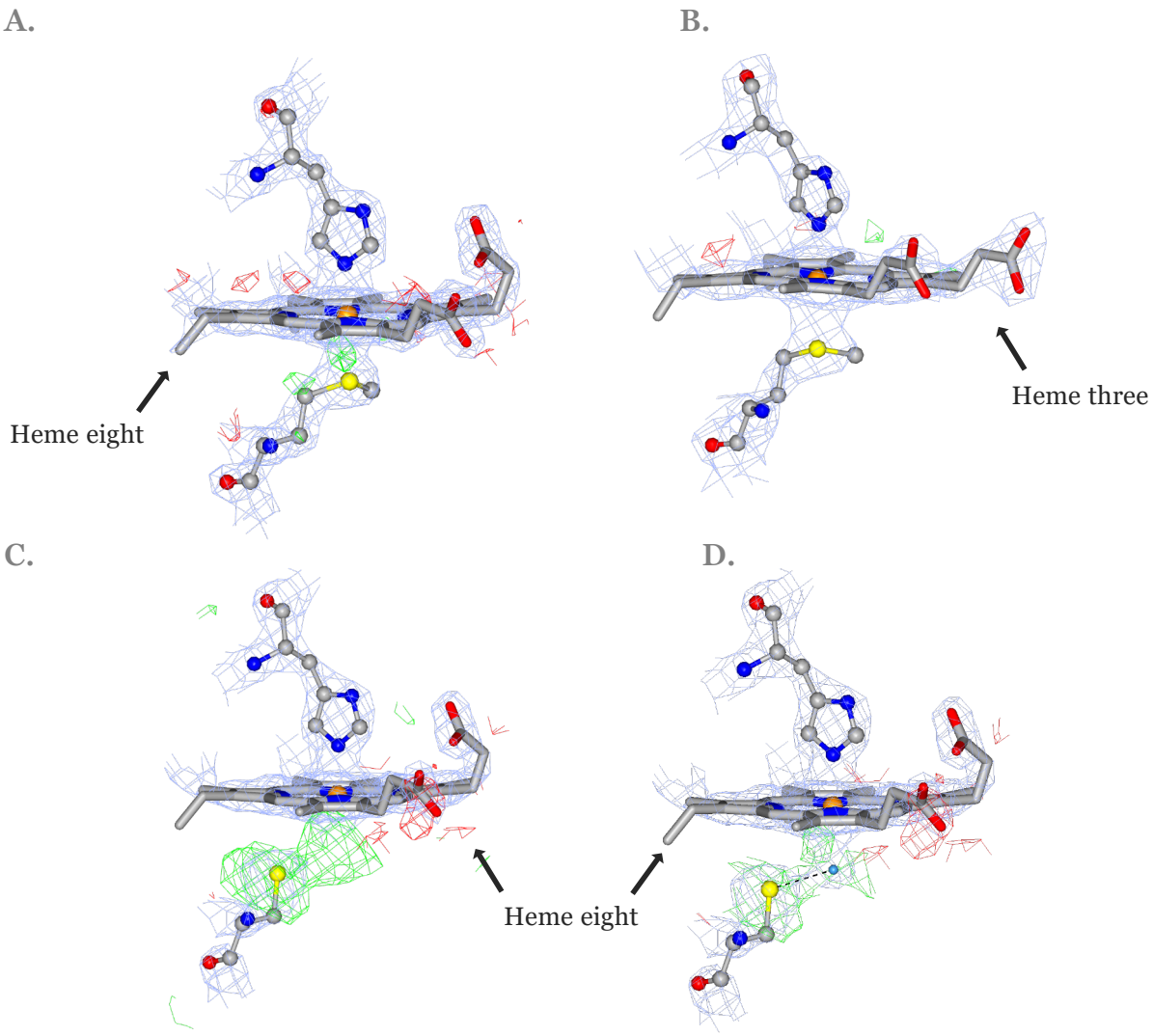

Figure 20. A) The structure of heme eight in $MtrC_{Sol}^{Y657C\ H561M}$. **B)** The structure of heme three in $MtrC_{Sol}^{Y657C\ H230M}$. **C)** The structure of heme eight in $MtrC_{Sol}^{Y657C\ H561C}$, showing a good fit for a cysteine but substantial missing density nearby and near the heme. **D)** The same as c), but with a water as a heme ligand, showing not enough density is offered by it, making it an unlikely candidate for ligation. A difference contour map (± 2.5 sigma) is shown where green is + 2.5 and red is - 2.5. Regular atom density maps are shown in light blue.

4.3 Protein film electrochemistry

Protein film electrochemistry was used to assess the redox properties of the proteins $MtrC_{Sol}^{Y657C}$, $MtrC_{Sol}^{Y657C\ H561M}$, $MtrC_{Sol}^{Y657C\ H561C}$, and $MtrC_{Sol}^{Y657C\ H230M}$. During cyclic voltammetry measurements a protein adsorbed working electrode has the voltage across it varied and the resulting current is recorded. The recorded data comes from two components, Faradaic and non-Faradaic contributions (55). The non-Faradaic component of the measurement comes from buildup and discharge of electrolytes in the electrode solution interface. This results in a baseline current that must be removed from all voltammograms to reveal the Faradaic current, the response due to electron exchange between the protein and electrode. In the proteins tested in this experiment there are ten hemes that can undergo a single electron reduction and oxidation reaction. Because there are 10× n=1 redox centres in each protein the trace observed on the voltammograms are a combination of all ten peaks.

Due to the difficulties associated with the de-convolution of cyclic voltammograms of multiheme cytochromes, fitting 10× n=1 redox centres to the graph was not attempted (56). Instead, a more generic assessment of the shape and form of the voltammogram was performed. Any major changes in shape of a normalised voltammogram will indicate changes in reduction potentials to one or more hemes in the structure.

All proteins studied show evidence of adhering to the ITO patch on the working electrode, as the natural white colour of the ITO patch turns pink after exposure to the protein solution, and retains this colour after washing. Furthermore, the protein adsorbed-ITO electrode shows redox activity between a potential window of +188 to −612 mV vs standard hydrogen electrode (SHE) as indicated by the negative trough (reduction processes) and positive peaks (oxidation processes). As seen in **Figure 21B** the general shape of the voltammogram trace for $MtrC_{Sol}^{Y657C}$ is comparable to that of literature data, with a distinct 'two peak' form (57). The trace for $MtrC_{Sol}^{Y657C\ H561M}$ appears to be missing a feature at +199 mV, reported to be characteristic of the protein due to the high potential centre created with a His/Met ligated heme (**Figure 21C**) (7). This however is a small feature and is

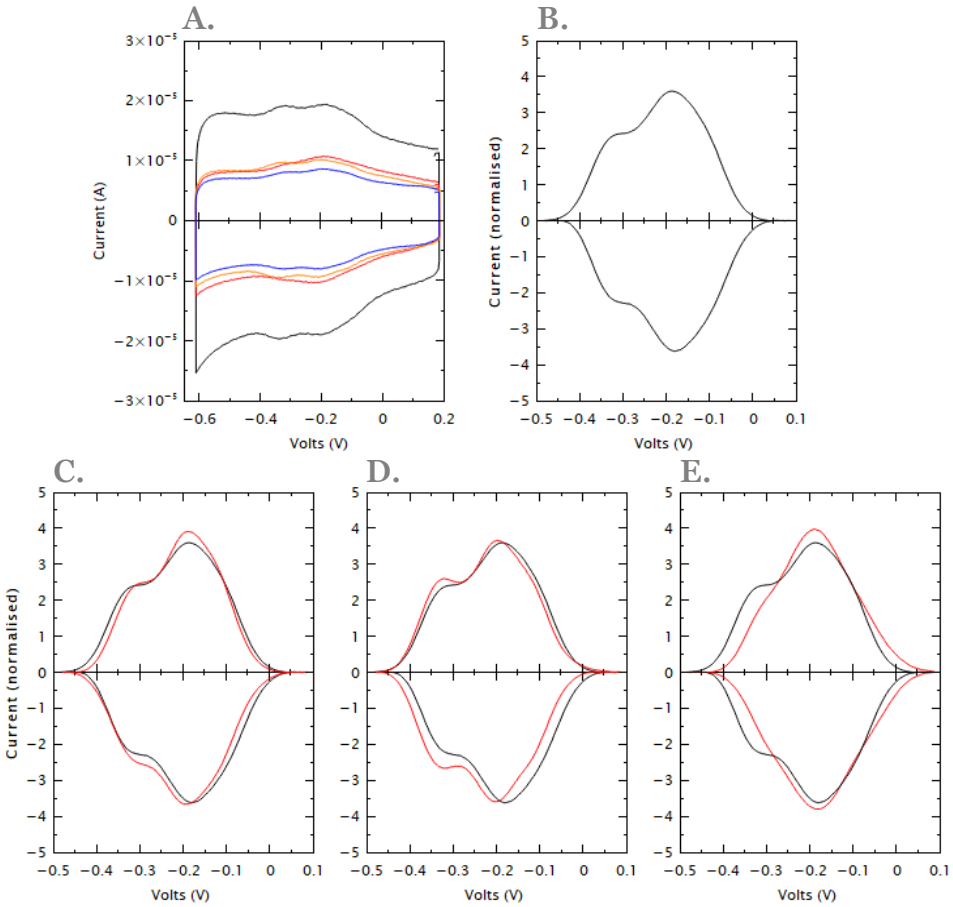

Figure 21. Protein film voltammograms. **A)** The measured cyclic voltammogram data collected from $MtrC_{Sol}^{Y657C}$ (black), $MtrC_{Sol}^{Y657C\ H561M}$ (blue), $MtrC_{Sol}^{Y657C\ H561C}$ (orange), and $MtrC_{Sol}^{Y657C\ H230M}$ (red). **B, C, D, &E)** all show the a trace for $MtrC_{Sol}^{Y657C}$ (black) as well as c, d, and e showing the traces for $MtrC_{Sol}^{Y657C\ H561M}$, $MtrC_{Sol}^{Y657C\ H561C}$, and $MtrC_{Sol}^{Y657C\ H230M}$ (all red) respectively. All traces are baseline corrected using the Q-SOAS software and normalised to the area under the curve. All measurements were performed while in 50 mM HEPES and 100 mM NaCl, pH 8.0 at a scan rate of 20 mV/s. All potentials quoted vs SHE.

possibly lost during baseline correction or due to the trace being of generally low intensity. The trace for $MtrC_{Sol}^{Y657C\ H230M}$ is potentially the most interesting as the characteristic two peak style of trace is almost completely lost (**Figure 21E**). This could be the result of one or more low reduction potential hemes shifting to more positive values, causing this secondary peak to diminish. The trace for $MtrC_{Sol}^{Y657C\ H561C}$ shows the opposite to $MtrC_{Sol}^{Y657C\ H230M}$ in the way it appears where the secondary peak appears to become more intense (**Figure 21D**). This is suggestive of one or more higher potential centres becoming more negative.

4.4 Summary

This chapter details the characterisation of two MtrC variants $MtrC_{Sol}^{Y657C\ H561C}$ and $MtrC_{Sol}^{Y657C\ H230M}$ using MCD, X-ray crystallography, and protein film electrochemistry. The results produced here have also revealed unknown information regarding the previously characterised MtrC variants $MtrC_{Sol}^{Y657C}$ and $MtrC_{Sol}^{Y657C\ H561M}$ in the form of their crystal structures.

The MCD spectra of $MtrC_{Sol}^{Y657C\ H561C}$ was typical of a low spin hemoprotein in both the reduced and oxidised form, as well as exhibiting no signs of any high spin heme. The X-ray crystallographic structure shows that no substitutions made have resulted in major structural changes, and nine of the ten hemes remain His/His coordinated. Introduction of a cysteine at position 561 in $MtrC_{Sol}^{Y657C\ H561C}$ appears to have resulted in heme eight being distally ligated not by a histidine, but by a group covalently attached to the introduced cysteine residue. This is supported by LC-MS data analysed in section 3.4, which shows the mass of $MtrC_{Sol}^{Y657C\ H561C}$ is +51 Da larger than expected. Protein film electrochemistry data shows that $MtrC_{Sol}^{Y657C\ H561C}$ adsorbs onto the ITO electrode, and shows redox activity within a potential window standard of $MtrC_{Sol}^{Y657C}$. When compared to $MtrC_{Sol}^{Y657C}$, $MtrC_{Sol}^{Y657C\ H561C}$ appears to have redox potential shifts towards more negative values, in line with expectations for a His/Cys ligated heme.

Similarly, the MCD spectra of $MtrC_{Sol}^{Y657C\ H230M}$ was also typical of a low spin hemoprotein in both the reduced and oxidised form, as well as exhibiting no signs of any high spin heme. No major structural changes were observed in the crystal structure, and again nine out the ten hemes remain His/His coordinated. However, the crystal structure also revealed that heme three was now coordinated by a methionine in a similar manner to $MtrC_{Sol}^{Y657C\ H230M}$, suggesting ligation by the introduced methionine at position 230 had occurred. Similarly, protein film electrochemistry data shows that $MtrC_{Sol}^{Y657C\ H230M}$ adsorbs onto the ITO electrode, and shows redox activity within a potential window standard of $MtrC_{Sol}^{Y657C}$. When compared to $MtrC_{Sol}^{Y657C}$, $MtrC_{Sol}^{Y657C\ H230M}$ appears to have redox potential shifts towards more positive values, in line with expectations for a His/Met ligated heme.

It should be noted that the ligand sets in the crystal structure have the potential to be different to those in solution, and further experiments will be needed to confirm the ligand set of the protein in solution. The X-ray crystallographic data collected here is the first time the structure of any $MtrC_{Sol}$ variant with the Y657C substitution has been resolved. The Y657C substitution has shown no discernible impact on overall protein fold in either $MtrC_{Sol}^{Y657C}$ or $MtrC_{Sol}^{Y657C\ H561M}$.

Chapter 5. Conclusions and future prospects

This thesis explored the possibility of engineering variants of the decaheme *c*-type cytochrome MtrC with non-canonical ligand sets with the objective of introducing spectrally unique hemes with differing redox potentials. This work aimed to produce three variants of MtrC, $MtrC_{Sol}^{Y657C\ H561C}$, $MtrC_{Sol}^{Y657C\ H230M}$, and $MtrC_{Sol}^{Y657C\ H230C}$. Of these targets both $MtrC_{Sol}^{Y657C\ H561C}$ and $MtrC_{Sol}^{Y657C\ H230M}$ have been successfully produced and characterised using a range of biochemical methods.

Evidence to show that both these MtrC variants contain ten low spin hemes has been provided, however the exact ligand set of each heme while the protein is in solution is yet to be described. There are several techniques that would report on the exact ligand set of the hemes in the proteins described here, however the use of these techniques is generally not suited to multiheme cytochromes. Electron paramagnetic resonance (EPR) measurements have been performed on MtrC, however these spectra were complex, coming from multiple magnetically coupled hemes (24). Deconvolution of such spectra would be difficult at best, and the presence of unknown ligand sets would likely make such a task formidable, and consequently it was not attempted. The technique best fit to MtrC would likely be near infra-red magnetic circular dichroism (NIR-MCD) spectroscopy. At the wavelengths for ligand charge transitions (>1800 nm) all heme ligands have a distinct 'fingerprint' that can be used to diagnose ligand set to the hemes of the protein. Helpfully, SoxAX has been described by NIR-MCD, and so ligand set determination of a heme with a Cys-SH ligand would be trivial (60).

The X-ray crystal structures of all MtrC variants were of high enough quality to produce a set of crystal structures and draw conclusions from them. However, not all data sets were of equal quality, especially those of $MtrC_{Sol}^{Y657C}$ and $MtrC_{Sol}^{Y657C\ H230M}$, which had noticeably worse resolutions when compared to $MtrC_{Sol}^{Y657C\ H561M}$ and $MtrC_{Sol}^{Y657C\ H561C}$. It is expected that higher quality diffraction data is easily attainable by collecting more data sets in attempts to simply find a crystal that provides better diffraction. If no crystals can be found to provide better diffraction, refining of growth conditions of the crystals would be possible.

Protein film electrochemical measurements provided in this thesis are preliminary results. These data sets have not yet been shown to be reproducible, and the results are not corroborated by other means of measuring redox potentials. Technical repeats of these experiments can be easily performed as the yields of the proteins support this. Results could then be complimented by potentiometric titration followed by UV-Vis electronic absorption spectroscopy, as performed by van Wonderan *et al.* on the $MtrC_{Sol}^{Y657C\ H561M}$ protein (7).

Unfortunately one of the protein targets for production, $MtrC_{Sol}^{Y657C\ H230C}$, was not successfully purified in this work. In light of the modification identified in the $MtrC_{Sol}^{Y657C\ H561C}$ protein, a hypothesis for the degradation of the $MtrC_{Sol}^{Y657C\ H230C}$ protein is that covalent modification to the introduced cysteine causes steric interference with protein folding. Although domain II and IV have high levels of homology they are not identical; small differences in the tertiary structure could cause the resulting protein to be unstable and intolerant to StrepTactin aided affinity chromatography. It is also worth considering the nature of the potential covalent modification to $MtrC_{Sol}^{Y657C\ H230C}$ may be different to that of $MtrC_{Sol}^{Y657C\ H561C}$. Evidence for a full length $MtrC_{Sol}^{Y657C\ H230C}$ protein was observed during expression trials. If a full length protein can be expressed, perhaps a different method of purification could be employed that does not cause the protein to degrade.

5.1 Consequences of the H561C substitution in $MtrC_{Sol}^{Y657C\ H561C}$

This work shows that $MtrC_{Sol}^{Y657C\ H561C}$ has been successfully purified and characterised. The ligand to heme eight in the crystal structure appear to be a covalent modification to the introduced cysteine at position 561, and evidence for the existence for this modification is supported by LC-MS data which show a mass increase of +51 Da. Covalent modifications to cysteine during the expression of hemoproteins is not a highly discussed area. Literature is available that discusses protection of free cysteines from the oxidising environment of the periplasm via formation of disulfide bridges with neighbouring cysteines (58). If neighbouring cysteines are not available then this disulfide bridge protection may not occur. This is reported to result in cysteine oxidation to sulphenic (Cys-OH), sulphinic (Cys-O_2H), and sulphonic (Cys-O_3H) acids, the latter of which is an irreversible in cells (59). The difference between the calculated and observed mass of $MtrC_{Sol}^{Y657C\ H561C}$ is +51 Da. Modification to a sulphinic acid should result in a mass increase of 32 Da, 19 Da less than the mass difference observed in . There are examples of proteins that have covalently modified cysteines as intended heme ligands, such as the SoxAX protein which has a His/Cys-SH ligand set (60, 61). The addition of a sulphur atom would unhelpfully result in the same mass increase as the addition of two oxygen atoms of 32 Da. However, the addition of three oxygen atoms (a sulphonic acid modification) would take the resulting covalent modification mass to a much closer 48 Da, only -3 Da mass difference between predicted and observed. This mass difference is within reasonable accuracy of the measurement.

The predicted mass of all proteins was calculated using a protonated heme mass of 615.17 Da (62). In a decaheme cytochrome, such as MtrC, even a small mass difference in a heme is multiplied by ten. Consequently, using the de-protonated mass of a heme would result in a predicted mass 20.0 Da lower than protonated. To eliminate this issue a trypsin digest of the protein followed by LC-MS analysis could identify individual residue masses. This would allow for greater accuracy in mass determination of individual residue mass within the protein and allow for identification of the covalent modification of the cysteine in $MtrC_{Sol}^{Y657C\ H561C}$. A brief look at the resolved crystal structure for $MtrC_{Sol}^{Y657C\ H561C}$ would dispute a sulphonic acid modification as the missing density does not appear to support three additional oxygen atoms. However, the structures presented here are a preliminary analysis, protein crystals that better diffract are thought to be obtainable, and a more rigorous refinement process of these structures could offer information currently unavailable.

5.2 Consequences of the H230M substitution in $MtrC_{Sol}^{Y657C\ H230M}$

Production and characterisation of the $MtrC_{Sol}^{Y657C\ H230M}$ protein was comparable to that of $MtrC_{Sol}^{Y657C\ H561C}$. The ligand to heme three in the crystal structure appears to be the methionine ligand introduced at position 230. The structure of heme three and its ligands is similar to the structure of heme eight in the already characterised $MtrC_{Sol}^{Y657C\ H561M}$ protein. His/Met ligated hemes have a small electronic charge transition absorbance at 695 nm. This charge transition is proposed to be detectable via UV-Vis electronic absorbance spectroscopy; however very high concentrations of protein are needed to detect this as it is a very weak transition. $MtrC_{Sol}^{Y657C\ H561M}$ contains a high potential centre that could be reduced using the mild reductant sodium ascorbate while all other hemes in the structure remained oxidised (7). Incubation of $MtrC_{Sol}^{Y657C\ H230M}$ with sodium ascorbate followed by UV-Vis electronic absorbance spectroscopy could reveal spectral features of a reduced heme.

5.3 Potential applications of the $MtrC_{Sol}^{Y657C\ H561C}$ and $MtrC_{Sol}^{Y657C\ H230M}$ proteins

In section 1.3 a figure is presented (**Figure 9**) that shows a schematic of MtrC acting as a photocatalyst. The following section discusses the potential of the $MtrC_{Sol}^{Y657C\ H561M}$ protein in stabilising excited electrons injected into the heme wire, and also presents the idea that the opposite could be achieved with $MtrC_{Sol}^{Y657C\ H561C}$ (i.e. an MtrC variant that stabilises the injection of an electron hole). Now that the $MtrC_{Sol}^{Y657C\ H561C}$ protein has been produced, the experiments to test these hypotheses are within reach. The preliminary protein film electrochemistry data suggests that the redox potential of one or more hemes in this protein have shifted to become more negative, however beam time at the central laser facility to perform pump-probe spectroscopy is certainly the best way to test the ideas presented here.

Since rates of reductive catalysis using photo excited electrons injected into the heme wire could be improved by increasing the charge separated lifetime, introduction of multiple high potential centres, i.e. a new protein $MtrC_{Sol}^{Y657C\ H561M\ H230M}$, could increase this charge separated lifetime, making it longer than already observed in the $MtrC_{Sol}^{Y657C\ H561M}$ protein alone. This could increase the value of the protein as a reductive catalyst by reducing unfavourable charge recombination with the photocatalyst.

Another opportunity presented by a domain II his/met heme is as a spectroscopic marker. As previously stated, the exact dynamics of electron transfer through the heme wire of MtrC was not known until very recently (7). Evidence was given to show electrons injected by a covalently attached $Ru(II)bipyridine_3$ dye into heme ten would transfer across heme nine to the his/met ligated heme eight (7). At this point in time the dynamics of electron transfer between domains IV and II of the protein is not clear. It is thought electron transfer between these domains could be interrupted though interface mutations. Measuring the success of disruption of electron transfer would be greatly aided by unique spectroscopic markers in both domains. A protein with a unique ligand set in each domain (i.e. $MtrC_{Sol}^{Y657C\ H561C\ H230M}$) would allow for experiments that tracked electron movement across the domains for MtrC by recording when hemes with known unique ligands sets become reduced and re-oxidise.

The ideas for experiments presented in this section are brief. The potential applications for the proteins produced in this thesis are limited to those of topics already being pursued by a small group of dedicated researchers. However, it is hoped that there is much potential for these proteins that is not considered here, and that the wider scientific community will take inspiration from the work done and produce results not yet thought to be possible.

References

1. Rossifanelli A, Antonini E, Caputo A. Hemoglobin and Myoglobin. Adv Protein Chem. 1964;19:73-222.
2. Liu X, Kim CN, Yang J, Jemmerson R, Wang X. Induction of apoptotic program in cell-free extracts: requirement for dATP and cytochrome c. Cell. 1996;86(1):147-57.
3. Hosler JP, Ferguson-Miller S, Mills DA. Energy transduction: proton transfer through the respiratory complexes. Annu Rev Biochem. 2006;75:165-87.
4. Bushnell GW, Louie GV, Brayer GD. High-resolution three-dimensional structure of horse heart cytochrome c. J Mol Biol. 1990;214(2):585-95.
5. Denisov IG, Makris TM, Sligar SG, Schlichting I. Structure and chemistry of cytochrome P450. Chem Rev. 2005;105(6):2253-77.
6. Gilles-Gonzalez MA, Gonzalez G. Heme-based sensors: defining characteristics, recent developments, and regulatory hypotheses. J Inorg Biochem. 2005;99(1):1-22.
7. van Wonderen JH, Adamczyk K, Wu X, Jiang X, Piper SEH, Hall CR, et al. Nanosecond heme-to-heme electron transfer rates in a multiheme cytochrome nanowire reported by a spectrally unique His/Met-ligated heme. Proc Natl Acad Sci U S A. 2021;118(39).
8. Myers CR, Nealson KH. Bacterial manganese reduction and growth with manganese oxide as the sole electron acceptor. Science. 1988;240(4857):1319-21.
9. Nealson KH, Saffarini D. Iron and manganese in anaerobic respiration: environmental significance, physiology, and regulation. Annu Rev Microbiol. 1994;48(1):311-43.
10. Venkateswaran K, Moser DP, Dollhopf ME, Lies DP, Saffarini DA, MacGregor BJ, et al. Polyphasic taxonomy of the genus Shewanella and description of Shewanella oneidensis sp. nov. Int J Syst Bacteriol. 1999;49(2):705-24.
11. Heidelberg JF, Paulsen IT, Nelson KE, Gaidos EJ, Nelson WC, Read TD, et al. Genome sequence of the dissimilatory metal ion-reducing bacterium Shewanella oneidensis. Nat Biotechnol. 2002;20(11):1118-23.
12. Breuer M, Rosso KM, Blumberger J, Butt JN. Multi-haem cytochromes in Shewanella oneidensis MR-1: structures, functions and opportunities. J R Soc Interface. 2015;12(102):20141117.
13. Myers CR, Myers JM. Cloning and sequence of cymA, a gene encoding a tetraheme cytochrome c required for reduction of iron(III), fumarate, and nitrate by Shewanella putrefaciens MR-1. J Bacteriol. 1997;179(4):1143-52.
14. McMillan DG, Marritt SJ, Butt JN, Jeuken LJ. Menaquinone-7 is specific cofactor in tetraheme quinol dehydrogenase CymA. J Biol Chem. 2012;287(17):14215-25.
15. Fonseca BM, Paquete CM, Neto SE, Pacheco I, Soares CM, Louro RO. Mind the gap: cytochrome interactions reveal electron pathways across the periplasm of Shewanella oneidensis MR-1. Biochem J. 2013;449(1):101-8.
16. Ross DE, Flynn JM, Baron DB, Gralnick JA, Bond DR. Towards electrosynthesis in shewanella: energetics of reversing the mtr pathway for reductive metabolism. PLoS One. 2011;6(2): e16649.
17. Tsapin AI, Vandenberghe I, Nealson KH, Scott JH, Meyer TE, Cusanovich MA, et al. Identification of a small tetraheme cytochrome c and a flavocytochrome c as two of the principal soluble cytochromes c in Shewanella oneidensis strain MR1. Appl Environ Microbiol. 2001;67(7):3236-44.
18. Hartshorne RS, Reardon CL, Ross D, Nuester J, Clarke TA, Gates AJ, et al. Characterization of an electron conduit between bacteria and the extracellular environment. Proc Natl Acad Sci U S A. 2009;106(52):22169-74.
19. Edwards MJ, White GF, Lockwood CW, Lawes MC, Martel A, Harris G, et al. Structural modeling of an outer membrane electron conduit from a metal-reducing bacterium suggests electron transfer via periplasmic redox partners. J Biol Chem. 2018;293(21):8103-12.
20. Edwards MJ, White GF, Butt JN, Richardson DJ, Clarke TA. The Crystal Structure of a Biological Insulated Transmembrane Molecular Wire. Cell. 2020;181(3):665-73 e10.
21. Beliaev AS, Saffarini DA. Shewanella putrefaciens mtrB encodes an outer membrane protein required for Fe(III) and Mn(IV) reduction. J Bacteriol. 1998;180(23):6292-7.
22. Schuetz B, Schicklberger M, Kuermann J, Spormann AM, Gescher J. Periplasmic electron transfer via the c-type cytochromes MtrA and FccA of Shewanella oneidensis MR-1. Appl Environ Microbiol. 2009;75(24):7789-96.

23. Beliaev AS, Saffarini DA, McLaughlin JL, Hunnicutt D. MtrC, an outer membrane decahaem c cytochrome required for metal reduction in Shewanella putrefaciens MR-1. Mol Microbiol. 2001;39(3):722-30.
24. Hartshorne RS, Jepson BN, Clarke TA, Field SJ, Fredrickson J, Zachara J, et al. Characterization of Shewanella oneidensis MtrC: a cell-surface decaheme cytochrome involved in respiratory electron transport to extracellular electron acceptors. J Biol Inorg Chem. 2007;12(7):1083-94.
25. Edwards MJ, White GF, Norman M, Tome-Fernandez A, Ainsworth E, Shi L, et al. Redox Linked Flavin Sites in Extracellular Decaheme Proteins Involved in Microbe-Mineral Electron Transfer. Sci Rep. 2015;5(1):11677.
26. Sanders C, Turkarslan S, Lee DW, Daldal F. Cytochrome c biogenesis: the Ccm system. Trends Microbiol. 2010;18(6):266-74.
27. Myers CR, Myers JM. The outer membrane cytochromes of Shewanella oneidensis MR-1 are lipoproteins. Lett Appl Microbiol. 2004;39(5):466-70.
28. Lockwood CWJ, van Wonderen JH, Edwards MJ, Piper SEH, White GF, Newton-Payne S, et al. Membrane-spanning electron transfer proteins from electrogenic bacteria: Production and investigation. Methods Enzymol. 2018;613:257-75.
29. Sandkvist M. Type II secretion and pathogenesis. Infect Immun. 2001;69(6):3523-35.
30. Shi L, Deng S, Marshall MJ, Wang Z, Kennedy DW, Dohnalkova AC, et al. Direct involvement of type II secretion system in extracellular translocation of Shewanella oneidensis outer membrane cytochromes MtrC and OmcA. J Bacteriol. 2008;190(15):5512-6.
31. Kranz RG, Richard-Fogal C, Taylor JS, Frawley ER. Cytochrome c biogenesis: mechanisms for covalent modifications and trafficking of heme and for heme-iron redox control. Microbiol Mol Biol Rev. 2009;73(3):510-28.
32. Owji H, Nezafat N, Negahdaripour M, Hajiebrahimi A, Ghasemi Y. A comprehensive review of signal peptides: Structure, roles, and applications. Eur J Cell Biol. 2018;97(6):422-41.
33. Costa TR, Felisberto-Rodrigues C, Meir A, Prevost MS, Redzej A, Trokter M, Waksman G. Secretion systems in Gram-negative bacteria: structural and mechanistic insights. Nat Rev Microbiol. 2015;13(6):343-59.
34. Teufel F, Almagro Armenteros JJ, Johansen AR, Gislason MH, Pihl SI, Tsirigos KD, et al. SignalP 6.0 predicts all five types of signal peptides using protein language models. Nat Biotechnol. 2022;40(7):1023-5.
35. Tsirigotaki A, De Geyter J, Sostaric N, Economou A, Karamanou S. Protein export through the bacterial Sec pathway. Nat Rev Microbiol. 2017;15(1):21-36.
36. Akopian D, Shen K, Zhang X, Shan SO. Signal recognition particle: an essential protein-targeting machine. Annu Rev Biochem. 2013;82(1):693-721.
37. Smithers L, Olatunji S, Caffrey M. Bacterial Lipoprotein Posttranslational Modifications. New Insights and Opportunities for Antibiotic and Vaccine Development. Front Microbiol. 2021;12:788445.
38. Fufezan C, Zhang J, Gunner MR. Ligand preference and orientation in b- and c-type heme-binding proteins. Proteins. 2008;73(3):690-704.
39. Zhuang J, Amoroso JH, Kinloch R, Dawson JH, Baldwin MJ, Gibney BR. Evaluation of electron-withdrawing group effects on heme binding in designed proteins: implications for heme a in cytochrome c oxidase. Inorg Chem. 2006;45(12):4685-94.
40. Eaves DJ, Grove J, Staudenmann W, James P, Poole RK, White SA, et al. Involvement of products of the nrfEFG genes in the covalent attachment of haem c to a novel cysteine-lysine motif in the cytochrome c552 nitrite reductase from Escherichia coli. Mol Microbiol. 1998;28(1):205-16.
41. Firer-Sherwood M, Pulcu GS, Elliott SJ. Electrochemical interrogations of the Mtr cytochromes from Shewanella: opening a potential window. J Biol Inorg Chem. 2008;13(6):849-54.
42. van Wonderen JH, Hall CR, Jiang X, Adamczyk K, Carof A, Heisler I, et al. Ultrafast Light-Driven Electron Transfer in a Ru(II)tris(bipyridine)-Labeled Multiheme Cytochrome. J Am Chem Soc. 2019;141(38):15190-200.
43. Piper SEH, Edwards MJ, van Wonderen JH, Casadevall C, Martel A, Jeuken LJC, et al. Bespoke Biomolecular Wires for Transmembrane Electron Transfer: Spontaneous Assembly of a Functionalized Multiheme Electron Conduit. Front Microbiol. 2021;12:714508.

44. Daff SN, Chapman SK, Turner KL, Holt RA, Govindaraj S, Poulos TL, Munro AW. Redox control of the catalytic cycle of flavocytochrome P-450 BM3. Biochemistry. 1997;36(45):13816-23.
45. Kappler U, Bernhardt PV, Kilmartin J, Riley MJ, Teschner J, McKenzie KJ, Hanson GR. SoxAX cytochromes, a new type of heme copper protein involved in bacterial energy generation from sulfur compounds. J Biol Chem. 2008;283(32):22206-14.
46. Reijerse EJ, Sommerhalter M, Hellwig P, Quentmeier A, Rother D, Laurich C, et al. The unusal redox centers of SoxXA, a novel c-type heme-enzyme essential for chemotrophic sulfur-oxidation of Paracoccus pantotrophus. Biochemistry. 2007;46(26):7804-10.
47. Jenner LP. Spectroscopic and electrochemical studies of di-heme thiosulphate dehydrogenases. UEA Digital Repository: University of East Anglia; 2019.
48. Berry EA, Trumpower BL. Simultaneous determination of hemes a, b, and c from pyridine hemochrome spectra. Anal Biochem. 1987;161(1):1-15.
49. Winter G, Lobley CM, Prince SM. Decision making in xia2. Acta Crystallogr D Biol Crystallogr. 2013;69:1260-73.
50. McCoy AJ, Grosse-Kunstleve RW, Adams PD, Winn MD, Storoni LC, Read RJ. Phaser crystallographic software. J Appl Crystallogr. 2007;40:658-74.
51. Muresan NM, Willkomm J, Mersch D, Vaynzof Y, Reisner E. Immobilization of a molecular cobaloxime catalyst for hydrogen evolution on a mesoporous metal oxide electrode. Angew Chem Int Ed Engl. 2012;51(51):12749-53.
52. Fourmond V, Hoke K, Heering HA, Baffert C, Leroux F, Bertrand P, Leger C. SOAS: a free program to analyze electrochemical data and other one-dimensional signals. Bioelectrochemistry. 2009;76(1-2):141-7.
53. Liu H, Naismith JH. An efficient one-step site-directed deletion, insertion, single and multiple-site plasmid mutagenesis protocol. BMC Biotechnol. 2008;8(1):91.
54. Marrit SJ, Kemp GL, Xiaoe L, Durrant JR, Cheesman MR, Butt JN. Spectrochemical characterization of a pentaheme cytochrome in solution and as electrocatalytically active films on nanocrystalline metal-oxide electrodes. J Am Chem Soc. 2008;130(27):8588-9.
55. Adamson H, Bond AM, Parkin A. Probing biological redox chemistry with large amplitude Fourier transformed ac voltammetry. Chem Commun (Camb). 2017;53(69):9519-33.
56. Protein film electrochemistry. Nature Reviews Methods Primers. 2023;3(1).
57. van Wonderen JH, Adamczyk K, Wu X, Jiang X, Piper SEH, Hall CR, et al. Nanosecond heme-to-heme electron transfer rates in a multiheme cytochrome nanowire reported by a spectrally unique His/Met-ligated heme. Proceedings of the National Academy of Sciences. 2021;118(39).
58. Depuydt M, Leonard SE, Vertommen D, Denoncin K, Morsomme P, Wahni K, et al. A periplasmic reducing system protects single cysteine residues from oxidation. Science. 2009;326(5956):1109-11.
59. Chung HS, Wang SB, Venkatraman V, Murray CI, Van Eyk JE. Cysteine oxidative posttranslational modifications: emerging regulation in the cardiovascular system. Circ Res. 2013;112(2):382-92.
60. Cheesman MR, Little PJ, Berks BC. Novel heme ligation in a c-type cytochrome involved in thiosulfate oxidation: EPR and MCD of SoxAX from Rhodovulum sulfidophilum. Biochemistry. 2001;40(35):10562-9.
61. Bamford VA, Bruno S, Rasmussen T, Appia-Ayme C, Cheesman MR, Berks BC, Hemmings AM. Structural basis for the oxidation of thiosulfate by a sulfur cycle enzyme. EMBO J. 2002;21(21):5599-610.
62. Yang F, Bogdanov B, Strittmatter EF, Vilkov AN, Gritsenko M, Shi L, et al. Characterization of purified c-type heme-containing peptides and identification of c-type heme-attachment sites in Shewanella oneidenis cytochromes using mass spectrometry. J Proteome Res. 2005;4(3):846-54.

Acknowledgements

First and foremost, I would like to thank Professor Julea Butt for her endless support and enthusiasm in my work, and for first introducing me to the world of scientific research. I would like to extend my thanks to Dr Colin Lockwood and Dr Jessica van Wonderen for their time and patience in teaching me laboratory skills and techniques that provided the foundations of this project's success. I would like to thank Dr Myles Cheesman for taking the time to show me how to run MCD, and for the use of his equipment. I would like to thank Dr Justin Bradley for his contribution to MCD, and to Antony Hinchliffe for going above and beyond in helping me with LC-MS.

I'd like to thank my fellow students Alexander Sutton-Cook for his help with PFE, Benjamin Nash for his help with protein crystallography, and Alejandro Morales Flórez for his help with all sorts of molecular biology. My thanks also go out to all other members of the BIO 2.30 lab for useful discussion and help in all varieties of topics.

I'd like to thank Professor Tom Clarke, Dr Amit Sachdeva, and Professor Andrew Hemmings for making up my supervisory team, and their resulting helpful discussion. I'd like to thank my examiners Dr David Swainsbury and Professor Jonathon Worral for taking time out of their schedules by agreeing to read and critique this work for me.

I'd like to thank my friends and family for their endless support. In particular, I'd like to thank Mum and Dad for their encouragement and for putting me on the road of science in the first place, and to my uncle Nigel for his critical sponsorship, without which I would have starved to death halfway through chapter 1 of this research.

Lastly, to my wife Holly, who has always insisted on me getting a tattoo in her honour, I say this...

Tattoos fade over time, a declaration of love on an academic document,
however, is substantially more permanent